IEEE Access
Multidisciplinary ⋮ Rapid Review ⋮ Open Access Journal

Received July 17, 2020, accepted July 26, 2020, date of publication July 29, 2020, date of current version August 11, 2020.

Digital Object Identifier 10.1109/ACCESS.2020.3012736

Channel Hardening in Cell-Free and User-Centric Massive MIMO Networks With Spatially Correlated Ricean Fading

ALBERTO ÁLVAREZ POLEGRE[1], (Student Member, IEEE), FELIP RIERA-PALOU[2], (Senior Member, IEEE), GUILLEM FEMENIAS[2], (Senior Member, IEEE), AND ANA GARCÍA ARMADA[1], (Senior Member, IEEE)

[1]Department of Signal Theory and Communications, Universidad Carlos III de Madrid, 28911 Madrid, Spain
[2]Mobile Communications Group, University of the Balearic Islands, 07122 Palma, Spain

Corresponding author: Alberto Álvarez Polegre (aalvarez@tsc.uc3m.es)

This work was supported in part by the Agencia Estatal de Investigación and Fondo Europeo de Desarrollo Regional (AEI/FEDER, UE), Ministerio de Economía y Competitividad (MINECO), Spain, through the project TERESA under Grant TEC2017-90093-C3-2-R and Grant TEC2017-90093-C3-3-R, and in part by the Spanish CDTI PID through the project OPALL5G: Optimization of Small Cells Performance in 5G NR.

ABSTRACT The irruption of the cell-free (CF) massive multiple-input multiple-output (MIMO) network topology has meant taking one step further the concept of massive MIMO as a means to provide uniform service in large coverage areas. A key property of massive MIMO networks is channel hardening, by which the channel becomes deterministic when the number of antennas grows large enough relative to the number of serviced users, easing the signal processing and boosting the performance of simple precoders. However, in CF massive MIMO, the fulfillment of this condition depends on several aspects that are not considered in classical massive MIMO systems. In this work, we address the presence of channel hardening in both CF massive MIMO and the recently appeared user-centric (UC) approach, under a spatially correlated Ricean fading channel using distributed and cooperative precoding and combining schemes and different power control strategies for both the downlink (DL) and uplink (UL) segments. We show that the line-of-sight (LOS) component, spatially correlated antennas and UC schemes have an impact on how the channel hardens. In addition, we examine the existent gap between the estimated achievable rate and the true network performance when channel hardening is compromised. Exact closed-form expressions for both the hardening metric and achievable DL/UL rates are given as well.

INDEX TERMS Cell-free, massive MIMO, user-centric, correlated Ricean fading, channel hardening.

I. INTRODUCTION

Universal frequency reuse has become the dominant planning strategy in cellular networks to maximize spectral efficiency, a condition imposed by the ever-increasing user data rate demands. Unfortunately, this comes at the cost of a large performance disparity between central and edge users that critically compromises fairness. Over the last decade a plethora of inter-cell interference coordination (ICIC) techniques, many of them relying on some form of cooperative processing (e.g., coordinated multi-point (CoMP)) have been proposed. Even though there have been several trials [1], [2], they have not been fully deployed in commercial networks.

Aiming at improving the per-user rate fairness among users in the coverage area, cell-free (CF) massive multiple-input multiple-output (MIMO) networks synergistically combine cooperative principles with one of the technological pillars of 5G, namely, massive MIMO [3]. First introduced by Ngo *et al.* in [4] (and further developed in [5]), a CF massive MIMO network consists of a large number of access points (APs) (base stations (BSs) in traditional cell-based networks) distributed over a large coverage area providing service coherently to a much smaller number of mobile stations (MSs) by means of linear precoding and combining.

The associate editor coordinating the review of this manuscript and approving it for publication was Jiayi Zhang.

APs are connected through a wired fronthaul link to a central processing unit (CPU) that plays the role of a network controller. Remarkably, by splitting the processing between the APs and the CPU, different trade-offs in terms of performance, complexity and fronthaul requirements can be realized. Though APs and MSs were first assumed to be single-antenna, in succeeding works, such as [6], [7], both entities were equipped with one or several antennas. Recently, different approaches derived from the original CF scheme have been proposed in which each AP only provides service to a subset of MSs based on a certain strategy. These alternative schemes were first proposed by Buzzi *et al.* in [8], where the criteria for an AP to provide service to a particular user was based on the channel strength between the given AP and the MS. These so-called user-centric (UC) approaches reduce considerably the fronthaul link traffic between each AP and the CPU, at the cost of a little performance loss.

In the classical multi-user MIMO schemes proposed in the late 2000s [9], computational complexity grew along the number of active users in the network and so did the training resources required to conduct the channel estimation at the receiver. In contrast, massive MIMO eases the way with linear processing thanks to the channel hardening phenomenon [3], by which small-scale fading effects vanish and time/frequency-selective channels behave basically as additive white Gaussian noise (AWGN) channels [10], [11]. Moreover, duplexing is typically implemented in the form of time division duplex (TDD), as after conducting the uplink (UL) channel estimation and deriving the corresponding precoder, channel hardening effectively removes almost all of the variability of the downlink (DL) channel. Relying on the massive MIMO inherited channel hardening property, most CF massive MIMO approaches are based on rather simple precoding and combining schemes, where performance analysis is carried out using analytical expressions mostly borrowed from the collocated massive MIMO literature. However, the CF massive MIMO scheme presents marked differences with respect to the classical massive MIMO scenario that in some cases, as it will be shown in this work, may compromise the validity of the analytical expressions.

A. PROBLEM STATEMENT AND RELATED WORK

As in massive MIMO, most of the CF related literature relies on the hardening property to derive the achievable rate bounds. However, it is often the case that only a small fraction of all APs contribute to the hardening and thus, the real network capacity can be considerably underestimated by the analytical achievable rate expressions. Moreover, in [12] it is shown that having instantaneous channel state information (CSI) at the user by including DL pilots, rather than relying on statistics, enhances the network performance making it closer to the perfect CSI case. As discussed in [13], increasing either the number of antennas per AP or the APs density, results in a stronger hardening effect. However, this work is limited to a simple precoding strategy without accounting for neither imperfect CSI nor pilot contamination, while assuming a spatially uncorrelated channel model. In addition, the possible effects that power allocation strategies may have on the channel hardening are omitted. The impact of these variables is analyzed in [14], where a channel hardening metric is given, namely, the channel hardening ratio. In this latter work, it is shown that the power allocation coefficients have indeed an impact on the degree of hardening achieved by the network, which in turn depends on the specific precoding strategy. Results show that as hardening increases, the gap between the capacity lower bounds and the date rates achieved under the assumption of perfect CSI at the receiver is reduced, highlighting the possible inaccuracy of the bounds inherited from collocated massive MIMO when hardening is compromised. Nonetheless, [14] considers distributed precoding schemes and heuristic power allocation control strategies only, while it did not address the UL segment. In addition, only a particular UC scheme was considered. Critically, both in [13], [14] an uncorrelated Rayleigh fading channel model was assumed, though practical channels in massive MIMO are in fact correlated [15] and often exhibit a line-of-sight (LOS) component. This is experimentally demonstrated in [16], where it is shown that the commonly used independent and identically distributed (i.i.d.) Rayleigh fading channel turns to be too optimistic in terms of channel hardening in practical scenarios and spatial correlation should be considered for avoiding misleading conclusions in theoretical works. Besides having spatially correlated antennas, in dense deployments, such as CF massive MIMO networks, the probability of having users close to an AP increases, which implies the existence of a dominant LOS component [17]. Considering spatial correlation and a LOS component in the link between an AP and a MS leads to a spatially correlated Ricean fading channel model. Spatially correlated Rayleigh fading channels were considered for CF massive MIMO in [18]–[21], whilst uncorrelated Ricean fading channels were examined in [17], [22]–[24], among others, though none of them have addressed the channel hardening phenomenon. In [25] a spatially correlated Ricean fading channel model is assumed, though pilot contamination is not considered and the UL segment is not addressed. Those contributions related to the UC approach, such as [8], [26], [27], are subject to i.i.d. Rayleigh fading channels. In addition, these works only consider a rather simple strategy when associating APs and MSs for service.

B. PAPER CONTRIBUTIONS

In this work we address and analyze the proposed metric in [14] under a realistic channel model and different system configurations. Our primary contributions can be summarized as follows:

- A CF massive MIMO system is assessed considering spatially correlated multi-antenna APs and the presence of a dominant LOS component. Distributed and cooperative signal processing is addressed for both DL and UL segments with different power allocation strategies. In addition, traditional CF scheme and several

UC approaches are considered under realistic operational conditions assuming pilot contamination and imperfect CSI.
- Exact closed-form expressions for computing both the channel hardening ratio and achievable user rates in the DL and UL segments are given for the distributed processing scenario. These expressions are validated through numerical results and Monte-Carlo simulations for different system configurations and parameters.
- The impact that spatial correlation, LOS component and UC strategies may have on the channel hardening ratio is analyzed and discussed.
- Achievable rates are compared with different proposed benchmarks. The existence of a gap between the achievable rates and the true network performance derived from the channel hardening ratio is discussed.

C. PAPER STRUCTURE AND NOTATION

The reminder of this work is organized as follows. Section II introduces the network structure, together with the spatially correlated Ricean fading channel model, the channel estimation process and the particularities if employing UC approaches. Building on this system model, Sections III and IV are devoted to describe and analyze the precoding and combining strategies under distributed and cooperative schemes, respectively. The channel hardening metric is shown in Section V for the DL and UL segments considering general and particular cases highlighting the differences between distributed and cooperative processing schemes. In order to demonstrate the effects that the different parameters have on the hardening ratio, a variety of capacity bounds are collected and summarized in Section VI against which the achievable rates can be compared to. DL and UL uniform and max-min power control strategies for either distributed or cooperative approaches are described in Section VII. In Section VIII, numerical results are presented and discussed. Finally, concluding remarks and future work are recapped in Section IX.

In this paper superscripts $\cdot^T$, $\cdot^*$, and $\cdot^H$ denote transpose, conjugate and conjugate transpose, respectively. Uppercase and lowercase bold symbols are used to denote matrices and vectors, respectively. The $\mathbb{E}\{\cdot\}$ and $\mathrm{Var}\{\cdot\}$ operators correspond to the expectation and variance, respectively, of the considered random variable (RV). The $\mathrm{diag}(\boldsymbol{A})$ operator denotes the column vector of the main diagonal of matrix $\boldsymbol{A}$, while the $\mathcal{D}(\boldsymbol{a})$ operator denotes a diagonal matrix with the elements of vector $\boldsymbol{a}$ at its main diagonal.

II. SYSTEM MODEL

Following the original CF massive MIMO proposal in [5], this paper considers a wireless communications system where M APs, each with N antennas conforming a uniform linear array (ULA), have been deployed over a large coverage area to simultaneously serve K single-antenna MSs on the same time-frequency resource. If instead of a pure CF scheme an alternative UC approach is considered, each AP will serve only a subset of users. Further details for these architectures are given in subsection II-C. As in most seminal works on this topic, all APs are connected to a CPU via fronthaul links. In this work, we do not address the possible limitations the fronthaul links may have. As stated in the introduction, DL and UL transmissions are organized in a TDD fashion whereby each coherence interval is split into three phases, namely, the UL training phase, the DL payload data transmission phase and the UL payload data transmission phase. In the UL training phase, all MSs transmit UL training pilots allowing the APs to estimate the propagation channels to/from those MSs to serve.[1] Subsequently, these channel estimates are used to compute the precoding and combining filters governing the DL payload data transmission and UL data detection.The training phase takes τ_p time-frequency samples from the τ_c samples available during the whole coherence interval. Note that it should hold that $\tau_c \geq \tau_p + \tau_d + \tau_u$, with τ_d and τ_u denoting the periods of the DL and UL payload phases measured in samples, respectively. Conveying CSI from AP to CPU can be avoided when using non-cooperative conjugate beamforming (CB) in the DL and matched filtering (MF) in the UL. In contrast, when relying on a centralized precoding technique, such as zero-forcing (ZF), APs should take care of uploading the locally collected estimates to the CPU to allow the calculation of the corresponding precoder and combiner [28].

A. CHANNEL MODEL

The classical i.i.d. Rayleigh fading propagation model used in most previous research works on CF massive MIMO networks (see, for instance [4], [5], [8], [27]–[30]) will be replaced by a simplified version of the third generation partnership project (3GPP) Urban Microcell model described in [31]. This model takes into account the possibility of the channel to toggle between non-line-of-sight (NLOS) and LOS and the existence of spatial correlation at the AP arrays.

Let us denote by β_{mk} the large-scale propagation losses of the link joining AP m and MS k, which can be expressed as $\beta_{mk} = 10^{\frac{-L_{mk}}{10}}$ with L_{mk} jointly representing the distance-dependent path loss and shadow fading defined as

$$L_{mk} = L_0 + 10\alpha \log_{10}(d_{mk}) + \chi_{mk}, \tag{1}$$

where L_0 is the path loss at a reference distance of 1 m, α is the environment-dependent path loss exponent and d_{mk} is the distance between AP m and MS k. These two coefficients may vary under LOS and NLOS conditions. On the other side, χ_{mk} corresponds to the shadow fading component modeled as a correlated log-normal RV with variance σ_χ^2 whose spatial correlation model is described in [5, (54)-(55)].

The resulting channel vector $\boldsymbol{g}_{mk} \in \mathbb{C}^{N\times 1}$ from the m-th AP to the k-th MS (including both large-scale and small-scale fading) can then be generically characterized as a Ricean fading channel consisting of a LOS component on top of

[1]Note that channel reciprocity can be exploited in TDD systems and therefore only UL pilots need to be transmitted.

a Rayleigh distributed component. That is,

$$\boldsymbol{g}_{mk} = \sqrt{\frac{K_{mk}}{K_{mk}+1}}\bar{\boldsymbol{h}}_{mk} + \sqrt{\frac{1}{K_{mk}+1}}\boldsymbol{h}_{mk}, \tag{2}$$

with

$$\bar{\boldsymbol{h}}_{mk} = \sqrt{\beta_{mk}}\left[1, e^{j\pi\sin\psi_{mk}}, \ldots, e^{j(N-1)\pi\sin\psi_{mk}}\right]^T, \tag{3}$$

being ψ_{mk} the angle of arrival (AoA) between AP m and MS k. The phase shift in (3) is assumed to remain constant during the coherence interval since APs are at fixed locations and MSs move slowly [17]. For later convenience we define

$$\tilde{\bar{\boldsymbol{h}}}_{mk} = \sqrt{\frac{K_{mk}}{K_{mk}+1}}\bar{\boldsymbol{h}}_{mk}. \tag{4}$$

The NLOS component $\boldsymbol{h}_{mk}$ follows a distribution $\mathcal{CN}(\boldsymbol{0}, \boldsymbol{R}_{mk})$ with $\boldsymbol{R}_{mk}$ representing the positive semi-definite spatial correlation matrix of the antenna array at AP m as seen from user k for a particular angular standard deviation (ASD) subject to $\mathrm{Tr}(\boldsymbol{R}_{mk}) = N\beta_{mk}$. Again, for convenience, we define

$$\tilde{\boldsymbol{R}}_{mk} = \frac{1}{K_{mk}+1}\boldsymbol{R}_{mk}. \tag{5}$$

Considering an AP antenna spacing of half wavelength, $\boldsymbol{R}_{mk}$ is defined as in [32, Chapter 2] with an AoA that follows a Gaussian distribution. Parameter K_{mk} denotes the Ricean K-factor, with $K_{mk} = 0$ for NLOS propagation links and $10\log_{10}(K_{mk}) \sim \mathcal{N}\left(\mu_K, \sigma_K^2\right)$ for LOS propagation links. The link between the m-th AP and the k-th MS will be considered to be in LOS with probability

$$p_{\mathrm{LOS}}(d_{mk}) = \min\left(1, \frac{d_0}{d_{mk}} + \left(1 - \frac{d_0}{d_{mk}}\right)e^{-\frac{d_{mk}}{2d_0}}\right), \tag{6}$$

where d_0 is a reference distance. The channel vector is distributed as

$$\boldsymbol{g}_{mk} \sim \mathcal{CN}\left(\tilde{\bar{\boldsymbol{h}}}_{mk}, \tilde{\boldsymbol{R}}_{mk}\right). \tag{7}$$

B. CHANNEL ESTIMATION

Communication in any coherence interval of a TDD-based massive MIMO system invariably starts with the MSs sending the pilot sequences to allow the channel to be estimated at the APs. During the UL training phase, all K MSs simultaneously transmit pilot sequences of τ_p samples to the APs and thus, the $N \times \tau_p$ received UL signal matrix at the m-th AP is given by

$$\boldsymbol{Y}_{p_m} = \sqrt{\tau_p\rho_p}\sum_{k=1}^{K}\boldsymbol{g}_{mk}\boldsymbol{\varphi}_k^T + \boldsymbol{N}_{p_m}, \tag{8}$$

where ρ_p is the normalized signal-to-noise ratio (SNR) of each pilot symbol, $\boldsymbol{\varphi}_k$ denotes the $\tau_p \times 1$ training sequence assigned to MS k, with $\|\boldsymbol{\varphi}_k\|^2 = 1$, and $\boldsymbol{N}_{p_m} \in \mathbb{C}^{N\times\tau_p}$ is a matrix of i.i.d. zero-mean circularly symmetric Gaussian RVs with unit variance. Ideally, training sequences should be chosen to be mutually orthogonal, however, since in most practical scenarios it holds that $K > \tau_p$, a given training sequence can be assigned to more than one MS, thus resulting in the so-called pilot contamination, a widely studied phenomenon in the context of collocated massive MIMO systems [3], [33], [34]. Some techniques for mitigating pilot contamination in a CF context have been proposed recently, for instance [35], [36]. In this work it is assumed that training sequences are assigned to MSs using the following procedure:

- In scenarios where $K \leq \tau_p$, MSs are always assigned mutually orthogonal sequences.
- In scenarios where $K > \tau_p$, the fingerprinting training introduced in [37] is applied. This technique ensures that pilot sequences are reused only among users which are located far apart from each other, hence reducing the pilot contamination effects (see [37, Section V] for details).

Considering scenarios where MSs move slowly, it is reasonable to assume that the Ricean K-factors K_{mk}, the LOS components $\bar{\boldsymbol{h}}_{mk}$, and the scatter fading correlation matrices $\boldsymbol{R}_{mk}$ change slowly and can be perfectly known at every AP for all users [17]. Under this assumption, we can define

$$\begin{aligned}\check{\boldsymbol{y}}_{p\,mk} &= \left(\boldsymbol{Y}_{p_m} - \mathbb{E}\left\{\boldsymbol{Y}_{p_m}\right\}\right)\boldsymbol{\varphi}_k^* \\ &= \sum_{k'=1}^{K}\sqrt{\frac{\tau_p\rho_p}{K_{mk'}+1}}\boldsymbol{h}_{mk'}\boldsymbol{\varphi}_{k'}^T\boldsymbol{\varphi}_k^* + \boldsymbol{N}_{p_m}\boldsymbol{\varphi}_k^*\end{aligned} \tag{9}$$

and

$$\check{\boldsymbol{g}}_{mk} = \boldsymbol{g}_{mk} - \mathbb{E}\left\{\boldsymbol{g}_{mk}\right\} = \sqrt{\frac{1}{K_{mk}+1}}\boldsymbol{h}_{mk}, \tag{10}$$

and then derive the minimum mean square error (MMSE) estimate for the channel between the k-th MS and the m-th AP as [17], [38]

$$\begin{aligned}\hat{\boldsymbol{g}}_{mk} &= \tilde{\bar{\boldsymbol{h}}}_{mk} + \frac{\mathbb{E}\left\{\check{\boldsymbol{y}}_{p\,mk}\check{\boldsymbol{g}}_{mk}^H\right\}}{\mathbb{E}\left\{\check{\boldsymbol{y}}_{p\,mk}\check{\boldsymbol{y}}_{p\,mk}^H\right\}}\check{\boldsymbol{y}}_{p\,mk} \\ &= \tilde{\bar{\boldsymbol{h}}}_{mk} + \sqrt{\tau_p\rho_p}\tilde{\boldsymbol{R}}_{mk}\boldsymbol{\Psi}_{mk}^{-1}\check{\boldsymbol{y}}_{p\,mk}\end{aligned} \tag{11}$$

where

$$\boldsymbol{\Psi}_{mk} = \tau_p\rho_p\sum_{k'=1}^{K}\tilde{\boldsymbol{R}}_{mk'}\left|\boldsymbol{\varphi}_{k'}^H\boldsymbol{\varphi}_k\right|^2 + \boldsymbol{I}_N. \tag{12}$$

Note that a particular AP needs to compute the channel estimates linking its serving MSs only. The channel estimate $\hat{\boldsymbol{g}}_{mk}$ and the MMSE channel estimation error $\boldsymbol{\epsilon}_{mk} = \boldsymbol{g}_{mk} - \hat{\boldsymbol{g}}_{mk}$ are random vectors distributed as

$$\hat{\boldsymbol{g}}_{mk} \sim \mathcal{CN}\left(\tilde{\bar{\boldsymbol{h}}}_{mk}, \boldsymbol{\Gamma}_{mk}\right), \tag{13}$$

and $\boldsymbol{\epsilon}_{mk} \sim \mathcal{CN}\left(\boldsymbol{0}, \boldsymbol{A}_{mk}\right)$, respectively, where

$$\boldsymbol{\Gamma}_{mk} = \tau_p\rho_p\tilde{\boldsymbol{R}}_{mk}\boldsymbol{\Psi}_{mk}^{-1}\tilde{\boldsymbol{R}}_{mk}^H \tag{14}$$

and

$$\boldsymbol{A}_{mk} = \mathbb{E}\left\{\boldsymbol{\epsilon}_{mk}\boldsymbol{\epsilon}_{mk}^H\right\} = \tilde{\boldsymbol{R}}_{mk} - \boldsymbol{\Gamma}_{mk}. \tag{15}$$

For later convenience, let us define at this point the $MN \times 1$ vector $\boldsymbol{g}_k = \left[\boldsymbol{g}_{1k}^T, \ldots, \boldsymbol{g}_{Mk}^T\right]^T$ as the vector collecting the

channel response from the M APs in the network to the k-th user and $\boldsymbol{g}_m = \left[\boldsymbol{g}_{m1}, \ldots, \boldsymbol{g}_{mK}\right]$ as the vector collecting the channel response from the K MSs to the m-th AP. Also, let us define the $MN \times K$ matrix $\boldsymbol{G} = \left[\boldsymbol{g}_1, \ldots, \boldsymbol{g}_K\right]$ as the whole system channel response matrix. Analogous relations can be established to define $\hat{\boldsymbol{g}}_k, \hat{\boldsymbol{g}}_m, \hat{\boldsymbol{G}}$ and $\boldsymbol{\epsilon}_k$.

C. AP-MS LINKING

When considering any clustering approach different from the pure CF scheme, a partial connectivity among the APs and the MSs must be established. To this end, let us define $\boldsymbol{C}$ as the $M \times K$ connectivity matrix, whose entries are given by [39]

$$c_{mk} = \begin{cases} 1, & \text{if AP } m \text{ serves MS } k \\ 0, & \text{otherwise.} \end{cases} \tag{16}$$

It is easy to check that conventional CF operation is attained by setting $c_{mk} = 1 \; \forall mk$. We note that c_{mk} coefficients are just a mathematical resource for easing the comprehension of the analysis throughout this work.

A particular strategy for designing $\boldsymbol{C}$ under a UC fashion first appeared in [8] where every AP only provides service to the K_{UC} MSs whose instantaneous estimated channels are the strongest, i.e., the largest $\|\hat{\boldsymbol{g}}_{mk}\|^2$. This particular strategy implies that APs must compute their c_{mk} coefficients within each coherence interval to account for the fast-changing small-scale fading channel components, thus limiting its practical application. In this work, the main criteria for linking an AP and a MS under any UC strategy will rely on the large-scale coefficient β_{mk} only, which is assumed to be known beforehand and whose variations take several coherence intervals. $\boldsymbol{C}$ will depend on the relative variations of the MSs large-scale channel components and will have, in general, a variation pace even slower than β_{mk}. Note that since channel hardening has been shown to clearly depend on the number of active APs in the network [14], designing $\boldsymbol{C}$ and studying how dense it needs to be becomes of cornerstone importance. We account for different β_{mk}-based clustering strategies to compare with the original CF scheme.

1) AP CENTRIC

Similar to initial proposal in [8], under this approach every AP will serve those K_{UC} MSs with largest β_{mk}. This strategy guarantees that no AP remains inactive in the network.

2) AP CENTRIC WITH MASTER AP

In AP centric scenario, though it is unlikely that any user will remain unserved if both APs and MSs are uniformly deployed, we cannot take this situation for granted in practical scenarios. In order to avoid this unwanted situation, the AP centric approach can be enhanced by assigning a *master* AP to each MS [40]. Under this approach every AP will serve K_{UC} MSs and will play the role of the *master* AP to a particular MS that may or may not be within the initial subset of K_{UC} MSs.

3) MS CENTRIC

Inversely to the AP centric approach, with the MS centric strategy the user will select those M_{UC} APs with stronger channels for being provided service with. In this scenario it is highly likely for several APs to remain inactive potentially resulting in a degradation of the overall system performance, so each AP will select the user with strongest channel to serve if it is not within any of the subsets of M_{UC} APs serving the MSs.

4) AP-MS CENTRIC

As a combination of the AP centric and MS centric strategies, in the AP-MS centric approach every MS will select its M_{UC} serving APs, while each AP will select its K_{UC} MSs subset. This mixed approach will generate much more fronthaul link data traffic than any other, but provides data rates close to the pure CF scheme. If compared to the rest of strategies, this scheme ensures a minimum of serving APs to a user (M_{UC}) and guarantees that every AP serves at least K_{UC} MSs.

III. DOWNLINK SIGNAL PROCESSING

Over the following paragraphs we address two different precoding strategies in the DL segment: distributed (non-cooperative) and centralized (cooperative). While in the first one there is no a priori need for the APs to share channel estimates with the CPU, in the centralized approach this becomes a mandatory action.

A. DISTRIBUTED PRECODING USING CB

When the DL transmitter processing is limited to some form of non-cooperative beamforming, suitably designed to incorporate the possibility of UC selective transmission in accordance to $\boldsymbol{C}$, the transmitted DL signal from AP m is given by

$$\boldsymbol{x}_m^{\text{CB}} = \sqrt{\rho_d} \sum_{k=1}^{K} \boldsymbol{\varpi}_{d,mk} s_{d,k} = \sqrt{\rho_d} \sum_{k=1}^{K} c_{mk} \sqrt{\eta_{mk}} \hat{\boldsymbol{g}}_{mk}^H s_{d,k}, \tag{17}$$

where $\rho_d = P_d/\sigma_d^2$ is the normalized DL SNR, $\boldsymbol{\varpi}_{d,mk} = c_{mk}\sqrt{\eta_{mk}}\hat{\boldsymbol{g}}_{mk}^H$ is the beamforming vector for the k-th MS and $s_{d,k}$ is the symbol transmitted to the k-th MS, which satisfies $\mathbb{E}\left\{\left|s_{d,k}\right|^2\right\} = 1$. Finally, η_{mk} is the power allocation coefficient that can be chosen in accordance to various criteria (see Section VII) but that nevertheless must fulfill an average power constraint at the m-th AP expressed as

$$\mathbb{E}\left\{\left\|\boldsymbol{x}_m^{\text{CB}}\right\|^2\right\} \leq \rho_d. \tag{18}$$

Under the assumption of single-antenna MSs, the estimated information symbol at the k-th MS is given by

$$\begin{aligned} \hat{s}_{d,k}^{\text{CB}} &= \sum_{m=1}^{M} \boldsymbol{x}_m^{\text{CB}} \boldsymbol{g}_{mk} + n_k \\ &= \sqrt{\rho_d} \sum_{m=1}^{M} \sum_{k'=1}^{K} c_{mk'} \sqrt{\eta_{mk'}} \hat{\boldsymbol{g}}_{mk'}^H \boldsymbol{g}_{mk} s_{d,k'} + n_k. \end{aligned} \tag{19}$$

where $n_k \sim \mathcal{CN}(0, 1)$ accounts for the receiver thermal noise. Now, assuming that only statistical CSI is available at the MSs (19) can be written as [5]

$$\hat{s}_{d,k}^{\mathrm{CB}} = \mathrm{DS}_{d,k}^{\mathrm{CB}} s_{d,k} + \mathrm{BU}_{d,k}^{\mathrm{CB}} s_{d,k} + \sum_{k' \neq k}^{K} \mathrm{UI}_{d,kk'}^{\mathrm{CB}} s_{d,k'} + n_k, \quad (20)$$

where

$$\mathrm{DS}_{d,k}^{\mathrm{CB}} \triangleq \sqrt{\rho_d}\mathbb{E}\left\{\sum_{m=1}^{M} \boldsymbol{\varpi}_{d,mk}\boldsymbol{g}_{mk}\right\}, \quad (21)$$

$$\mathrm{BU}_{d,k}^{\mathrm{CB}} \triangleq \sqrt{\rho_d}\left(\sum_{m=1}^{M} \boldsymbol{\varpi}_{d,mk}\boldsymbol{g}_{mk} - \mathbb{E}\left\{\sum_{m=1}^{M} \boldsymbol{\varpi}_{d,mk}\boldsymbol{g}_{mk}\right\}\right), \quad (22)$$

and

$$\mathrm{UI}_{d,kk'}^{\mathrm{CB}} \triangleq \sqrt{\rho_d}\sum_{m=1}^{M} \boldsymbol{\varpi}_{d,mk'}\boldsymbol{g}_{mk} \quad (23)$$

are defined as the strength of the desired signal, the beamforming gain uncertainty, and the interference caused by the transmission to the k'-th MS, respectively. Closed-form expressions for these terms are given in Sections V and VI.

B. COOPERATIVE PRECODING USING ZF

If short-term cooperation between APs and the CPU is allowed, the classical MIMO ZF precoding technique, first recast in the context of the CF architecture in [28], is considered. This strategy, taking into account the connectivity matrix $\boldsymbol{C}$, results in the computation of the ZF precoding matrix

$$\boldsymbol{W} = \hat{\boldsymbol{G}}_c^* \left(\hat{\boldsymbol{G}}_c^T \hat{\boldsymbol{G}}_c^*\right)^{-1}, \quad (24)$$

where $\hat{\boldsymbol{G}}_c = \hat{\boldsymbol{G}} \odot \boldsymbol{C}$ with $\odot$ denoting the element-wise product serving to take into account the specific AP-MS connectivity of the network.[2] The overall $MN \times 1$ precoded vector is then defined as

$$\boldsymbol{x}^{\mathrm{ZF}} = \boldsymbol{W}\boldsymbol{\Omega}\boldsymbol{s}_d, \quad (25)$$

where $\boldsymbol{s}_d$ is the $K \times 1$ vector of DL user information symbols and $\boldsymbol{\Omega} = \mathcal{D}\left(\left[\sqrt{\omega_1}, \ldots, \sqrt{\omega_K}\right]\right)$ is a $K \times K$ diagonal power allocation matrix with each element ω_k representing the power coefficient assigned to MS k. As in the distributed case, power allocation coefficients should be computed to satisfy a prescribed maximum power constraint. The received signal at the k-th MS is

$$\begin{aligned}\hat{s}_{d,k}^{\mathrm{ZF}} &= \sqrt{\rho_d}\boldsymbol{g}_k^T \boldsymbol{x}^{\mathrm{ZF}} + n_k \\ &= \sqrt{\rho_d}\left(\hat{\boldsymbol{g}}_k + \boldsymbol{\epsilon}_k\right)^T \hat{\boldsymbol{G}}_c^* \left(\hat{\boldsymbol{G}}_c^T \hat{\boldsymbol{G}}_c^*\right)^{-1} \boldsymbol{\Omega}\boldsymbol{s}_d + n_k \\ &= \sqrt{\rho_d\omega_k}s_{d,k} + \underbrace{\sqrt{\rho_d}\boldsymbol{\epsilon}_k^T \hat{\boldsymbol{G}}_c^* \left(\hat{\boldsymbol{G}}_c^T \hat{\boldsymbol{G}}_c^*\right)^{-1} \boldsymbol{\Omega}\boldsymbol{s}_d}_{\mathrm{EN}_{d,k}} + n_k, \end{aligned} \quad (26)$$

where the first term is the desired signal, the second term accounts for the imperfect CSI and errors derived from the fact of not inverting the whole channel matrix (UC scenarios, treated as effective noise) and n_k is the receiver's thermal noise. Note that whereas CB can be implemented both in a centralized (at the CPU) or distributed manner (at the APs),[3] the ZF technique can only be applied at the CPU since the precoder calculation requires knowledge of the CSI between all of the MSs and their serving APs (in accordance to $\boldsymbol{C}$).

IV. UPLINK SIGNAL PROCESSING

The UL combining operation will follow again distributed and cooperative processing schemes. In the same fashion as in the DL segment, the distributed combiner will consist of a MF performed locally at each AP, whilst the cooperative scheme will be based on the ZF processing performed at the CPU. In this work, we assume the same UC strategy for both the DL and UL segment. Nevertheless, upcoming analysis is agnostic of either the followed UC strategy or any particular value of c_{mk}.

A. DISTRIBUTED COMBINING USING MF

Under the distributed combining strategy, all MSs send their corresponding data symbols $s_{u,k}$ satisfying $\mathbb{E}\left\{\left|s_{u,k}\right|^2\right\} = 1$, which are received by every AP in the network. The received UL data payload signal at the m-th AP is

$$\boldsymbol{y}_m^{\mathrm{MF}} = \sqrt{\rho_u}\sum_{k=1}^{K}\sqrt{\eta_k}\boldsymbol{g}_{mk}s_{u,k} + \boldsymbol{n}_m, \quad (27)$$

where $\rho_u = P_u/\sigma_u^2$ is the normalized UL SNR, η_k corresponds to the power control coefficient subject to $0 \leq \eta_k \leq 1$ and $\boldsymbol{n}_m$ is the noise vector following a $\mathcal{CN}(0, \boldsymbol{I}_N)$ distribution accounting for the thermal noise at the m-th AP. Each AP will apply MF to the received signal with the combining vector $\boldsymbol{\varpi}_{u,mk} = c_{mk}\hat{\boldsymbol{g}}_{mk}^H$ and will send it to the CPU through the fronthaul link connection where $s_{u,k}$ is detected from $\hat{s}_{u,k}^{\mathrm{MF}}$. This whole operation is expressed as

$$\begin{aligned}\hat{s}_{u,k}^{\mathrm{MF}} &= \sum_{m=1}^{M}\boldsymbol{\varpi}_{u,mk}\boldsymbol{y}_m^{\mathrm{MF}} = \sum_{m=1}^{M} c_{mk}\hat{\boldsymbol{g}}_{mk}^H \boldsymbol{y}_m^{\mathrm{MF}} \\ &= \sqrt{\rho_u}\sum_{k'=1}^{K}\sqrt{\eta_{k'}}\sum_{m=1}^{M} c_{mk}\hat{\boldsymbol{g}}_{mk}^H \boldsymbol{g}_{mk'}s_{u,k'} \\ &\quad + \sum_{m=1}^{M} c_{mk}\hat{\boldsymbol{g}}_{mk}^H \boldsymbol{n}_m. \end{aligned} \quad (28)$$

Similarly to the DL scenario, the $\hat{s}_{u,k}^{\mathrm{MF}}$ symbol can be expressed as a linear combination of $\mathrm{DS}_{u,k}^{\mathrm{MF}}$, $\mathrm{BU}_{u,k}^{\mathrm{MF}}$ and $\mathrm{UI}_{u,kk'}^{\mathrm{MF}}$. Even though APs have the instantaneous channel

[2] Note that when using UC approaches, matrix $\hat{\boldsymbol{G}}_c$ will typically be sparse, in which case efficient algorithms can be applied to compute the pseudoinverse in (24) [41].

[3] When infinite capacity fronthaul links between the APs and MSs are considered, centralized and distributed implementation of the CB are mathematically equivalent. In contrast, when limited-capacity fronthauls are considered, the centralized and distributed implementations of these two algorithms differ dramatically.

estimates, these are not forwarded to any other entity, so only statistical CSI is assumed to be available at the CPU [5]. Consequently

$$\hat{s}_{u,k}^{\mathrm{MF}} = \mathrm{DS}_{u,k}^{\mathrm{MF}} s_{u,k} + \mathrm{BU}_{u,k}^{\mathrm{MF}} s_{u,k} + \sum_{k' \neq k}^{K} \mathrm{UI}_{u,kk'}^{\mathrm{MF}} s_{u,k'} + \mathrm{NT}_{u,k}^{\mathrm{MF}}, \tag{29}$$

where

$$\mathrm{DS}_{u,k}^{\mathrm{MF}} \triangleq \sqrt{\rho_d \eta_k}\, \mathbb{E}\left\{ \sum_{m=1}^{M} \boldsymbol{\varpi}_{u,mk} \boldsymbol{g}_{mk} \right\}, \tag{30}$$

$$\mathrm{BU}_{u,k}^{\mathrm{MF}} \triangleq \sqrt{\rho_d \eta_k} \left(\sum_{m=1}^{M} \boldsymbol{\varpi}_{u,mk} \boldsymbol{g}_{mk} \mathbb{E}\left\{ \sum_{m=1}^{M} \boldsymbol{\varpi}_{u,mk} \boldsymbol{g}_{mk} \right\} \right), \tag{31}$$

$$\mathrm{UI}_{u,kk'}^{\mathrm{MF}} \triangleq \sqrt{\rho_d \eta_{k'}} \sum_{m=1}^{M} \boldsymbol{\varpi}_{u,mk} \boldsymbol{g}_{mk'}, \tag{32}$$

and

$$\mathrm{NT}_{u,k}^{\mathrm{MF}} \triangleq \mathbb{E}\left\{ \sum_{m=1}^{M} \boldsymbol{\varpi}_{u,mk} \boldsymbol{g}_{mk} \right\} \tag{33}$$

are defined as the strength of the desired signal, the beamforming gain uncertainty, the interference caused by the reception from the k'-th MS, and the noise term, respectively. Closed-form expressions for these terms are given in Sections V and VI.

B. COOPERATIVE COMBINING USING ZF

In similar fashion as in the DL segment, the UL cooperative combining holds as follows. The collective signal received at the APs sent from all MSs is defined as

$$\boldsymbol{y}^{\mathrm{ZF}} = \sqrt{\rho_u} \boldsymbol{G} \boldsymbol{\Theta} \boldsymbol{s}_u + \boldsymbol{n} = \sqrt{\rho_u} \sum_{k=1}^{K} \sqrt{\theta_k} \boldsymbol{g}_k s_{u,k} + \boldsymbol{n}, \tag{34}$$

where $\boldsymbol{\Theta} = \mathcal{D}\left(\left[\sqrt{\theta_1}, \ldots, \sqrt{\theta_K}\right]\right)$ is a $K \times K$ diagonal power allocation matrix with each element θ_k representing the power coefficient assigned to MS k and $\boldsymbol{n} \in \mathbb{C}^{MN \times 1}$ is the vector accounting for thermal noise at all the APs. The entries of $\boldsymbol{y}^{\mathrm{ZF}}$ are forwarded from each AP to the CPU for detecting the corresponding set of data symbols as

$$\begin{aligned} \hat{\boldsymbol{s}}_u^{\mathrm{ZF}} &= \boldsymbol{W}^T \boldsymbol{y}^{\mathrm{ZF}} = \sqrt{\rho_u} \boldsymbol{\Theta} \boldsymbol{W}^T \boldsymbol{G} \boldsymbol{s}_u + \boldsymbol{W}^T \boldsymbol{n} \\ &= \sqrt{\rho_u} \boldsymbol{P} \boldsymbol{s}_u + \sqrt{\rho_u} \boldsymbol{\Theta} \boldsymbol{W}^T \boldsymbol{E} \boldsymbol{s}_u + \boldsymbol{W}^T \boldsymbol{n}, \end{aligned} \tag{35}$$

where $\boldsymbol{E} = [\boldsymbol{\epsilon}_1, \ldots, \boldsymbol{\epsilon}_K]$. Each component of $\hat{\boldsymbol{s}}_u^{\mathrm{ZF}}$ is combined as

$$\hat{s}_{u,k}^{\mathrm{ZF}} = \sqrt{\rho_u \theta_k} s_{u,k} + \underbrace{\sqrt{\rho_u \theta_k} \boldsymbol{w}_k^T \boldsymbol{\epsilon}_k}_{\mathrm{EN}_{u,k}} s_{u,k} + r_k, \tag{36}$$

where r_k is the k-th entry of the vector $\boldsymbol{W}^T \boldsymbol{n}$. In this expression the first term represents the useful signal and the second term represents the combined effects of imperfect CSI and the matrix inversion errors being $\boldsymbol{w}_k$ the k-th column vector of matrix $\boldsymbol{W}$.

V. CHANNEL HARDENING RATIO

The concept of channel hardening first gained importance in the context of conventional (i.e., cell-based) massive MIMO systems, when it was shown that the time/frequency-selectivity of the channel vanishes as the number of antennas grows large [3]. Under such condition, MSs can rely on channel statistics rather than on their instantaneous channel gains when estimating the DL achievable rates and conducting the optimization of certain network parameters (e.g., pilot sequence assignment, calculation of power allocation coefficients). This effect, together with the channel reciprocity given by TDD communications, eliminates the necessity of having any form of DL pilots. As channel estimation is performed locally at each AP and does not need to be forwarded necessarily (unless a cooperative processing is implemented, such as ZF) to the CPU, the UL achievable rates estimation would rely as well on statistical CSI knowledge. In the specific scenario of collocated massive MIMO under CB/MF processing and perfect CSI knowledge, one can mathematically express the channel hardening effect as [13]

$$\frac{\|\boldsymbol{g}_k\|^2}{\mathbb{E}\left\{\|\boldsymbol{g}_k\|^2\right\}} \longrightarrow 1, \quad \text{as } N \longrightarrow \infty, \tag{37}$$

being $\|\boldsymbol{g}_k\|^2$ the effective channel gain between the k-th user and all antennas from a particular AP [32], if referring to the DL segment. Note that the instantaneous equivalent channel converges to its mean when transmission takes place from a large number of antennas. However, in a CF massive MIMO scenario, the total number of antennas (MN) is not the only factor that affects the channel hardening. As it is shown in the following paragraphs, there are several parameters that contribute positively or negatively on how the channel hardens. First, let us generalize (37) for accounting for the effects of power allocation, imperfect CSI and a specific precoder/combiner scheme. We may rewrite (37) as

$$\frac{|\boldsymbol{\varpi}_k \boldsymbol{g}_k|}{\mathbb{E}\left\{|\boldsymbol{\varpi}_k \boldsymbol{g}_k|\right\}} \longrightarrow 1, \quad \text{as } M, N \longrightarrow \infty, \tag{38}$$

where $|\boldsymbol{\varpi}_k \boldsymbol{g}_k|$ represents the joint propagation channel gain with $\boldsymbol{\varpi}_k = \left[\boldsymbol{\varpi}_{a,1k}, \cdots, \boldsymbol{\varpi}_{a,Mk}\right]$ and $a \in [d, u]$ being a token to denote either DL or UL. Based on this latter expression, from this point onward we define the channel hardening ratio for an arbitrary user k as [14]

$$\xi_k = \mathrm{Var}\left\{ \frac{|\boldsymbol{\varpi}_k \boldsymbol{g}_k|}{\mathbb{E}|\boldsymbol{\varpi}_k \boldsymbol{g}_k|} \right\} = \frac{\mathbb{E}\left\{|\boldsymbol{\varpi}_k \boldsymbol{g}_k|^2\right\} - \mathbb{E}\left\{|\boldsymbol{\varpi}_k \boldsymbol{g}_k|\right\}^2}{\mathbb{E}\left\{|\boldsymbol{\varpi}_k \boldsymbol{g}_k|\right\}^2}. \tag{39}$$

Note that this expression is valid for both DL and UL segments, differing only on the power control and connectivity coefficients. The convergence of this ratio to zero implies that the instantaneous joint propagation channel vector is close to its mean and thus a high degree of channel hardening is achieved. In other words, the channel hardening ratio essentially measures how deterministic a wireless link is, i.e. having a low hardening ratio would mean this link is quasi-deterministic. Furthermore, achieving a certain channel

hardening ratio has an impact on the accuracy of estimated achievable rates, which will be addressed later on. We also note that (39) was first analyzed in detail in [13] for the case of CB but, however, rather unrealistic conditions were considered (i.e., perfect CSI, no pilot contamination and uncorrelated Rayleigh fading channel model). In the next section we revisit this problem, among other particular cases, to account for the impact of imperfect CSI, correlation between antennas and the Ricean component contribution. Connectivity coefficients are shown to have a significant impact on channel hardening when implementing UC approaches.

A. HARDENING RATIO WITH DISTRIBUTED PROCESSING

Building on (21) and (22), the DL hardening ratio can be found to be

$$\begin{aligned}\xi_{d,k}^{\mathrm{CB}} &= \frac{\mathbb{E}\left\{\left|\mathrm{BU}_{d,k}^{\mathrm{CB}}\right|^2\right\}}{\left|\mathrm{DS}_{d,k}^{\mathrm{CB}}\right|^2} \\ &= \frac{\sum_{m=1}^{M}\mathbb{E}\left\{\left|\boldsymbol{\varpi}_{d,mk}\boldsymbol{g}_{mk}-\mathbb{E}\left\{\left|\boldsymbol{\varpi}_{d,mk}\boldsymbol{g}_{mk}\right|\right\}\right|^2\right\}}{\left(\sum_{m=1}^{M}\mathbb{E}\left\{\left|\boldsymbol{\varpi}_{d,mk}\boldsymbol{g}_{mk}\right|\right\}\right)^2} \\ &= \frac{\sum_{m=1}^{M}c_{mk}\eta_{mk}\mathbb{E}\left\{\left|\hat{\boldsymbol{g}}_{mk}^H\boldsymbol{g}_{mk}-\mathbb{E}\left\{\left|\hat{\boldsymbol{g}}_{mk}^H\boldsymbol{g}_{mk}\right|\right\}\right|^2\right\}}{\left(\sum_{m=1}^{M}c_{mk}\sqrt{\eta_{mk}}\mathbb{E}\left\{\left|\hat{\boldsymbol{g}}_{mk}^H\boldsymbol{g}_{mk}\right|\right\}\right)^2} \\ &= \frac{\sum_{m=1}^{M}c_{mk}\eta_{mk}\left(\mathbb{E}\left\{\left|\hat{\boldsymbol{g}}_{mk}^H\boldsymbol{g}_{mk}\right|^2\right\}-\mathbb{E}\left\{\left|\hat{\boldsymbol{g}}_{mk}^H\boldsymbol{g}_{mk}\right|\right\}^2\right)}{\left(\sum_{m=1}^{M}c_{mk}\sqrt{\eta_{mk}}\mathbb{E}\left\{\left|\hat{\boldsymbol{g}}_{mk}^H\boldsymbol{g}_{mk}\right|\right\}\right)^2} \\ &\overset{(a)}{=} \frac{\sum_{m=1}^{M}c_{mk}\eta_{mk}\left(2\tilde{\bar{\boldsymbol{h}}}_{mk}^H\boldsymbol{\Gamma}_{mk}\tilde{\bar{\boldsymbol{h}}}_{mk}+\mathrm{Tr}\left(\tilde{\boldsymbol{R}}_{mk}\boldsymbol{\Gamma}_{mk}\right)\right)}{\left(\sum_{m=1}^{M}c_{mk}\sqrt{\eta_{mk}}\left(\tilde{\bar{\boldsymbol{h}}}_{mk}^H\tilde{\bar{\boldsymbol{h}}}_{mk}+\mathrm{Tr}(\boldsymbol{\Gamma}_{mk})\right)\right)^2}. \end{aligned} \tag{40}$$

Note that and expectation operators are taken with respect to the small-scale fading channel variations. Recalling (7) and (13) and knowing that $\hat{\boldsymbol{g}}_{mk}=\boldsymbol{g}_{mk}+\boldsymbol{\epsilon}_{mk}$ and $\hat{\boldsymbol{g}}_{mk}$ and $\boldsymbol{\epsilon}_{mk}$ are mutually uncorrelated thanks to MMSE channel estimation, in the last equality (a) we have uased a particularization of [42, Lemma 5] expressed as

$$\begin{aligned}&\mathbb{E}\left\{\left|\boldsymbol{q}^H\boldsymbol{B}\boldsymbol{q}\right|^2\right\} \\ &\quad=\left|\mathrm{Tr}\left(\boldsymbol{R}_q\boldsymbol{B}\right)\right|^2+\mathrm{Tr}\left(\boldsymbol{R}_q\boldsymbol{B}\boldsymbol{R}_q\boldsymbol{B}^H\right)+\left|\bar{\boldsymbol{q}}^H\boldsymbol{B}\bar{\boldsymbol{q}}\right|^2 \\ &\qquad+2\Re\left\{\bar{\boldsymbol{q}}^H\boldsymbol{B}\bar{\boldsymbol{q}}\mathrm{Tr}\left(\boldsymbol{R}_q\boldsymbol{B}^H\right)\right\}+2\Re\left\{\bar{\boldsymbol{q}}^H\boldsymbol{B}\boldsymbol{R}_q\boldsymbol{B}^H\bar{\boldsymbol{q}}\right\}, \end{aligned} \tag{41}$$

where $\boldsymbol{q}\sim\mathcal{CN}\left(\bar{\boldsymbol{q}},\boldsymbol{R}_q\right)$ and $\boldsymbol{B}$ is a deterministic matrix.

Following similar computation as in (40), it is easy to check that the channel hardening ratio for the UL segment is given by

$$\begin{aligned}\xi_{u,k}^{\mathrm{MF}} &= \frac{\mathbb{E}\left\{\left|\mathrm{BU}_{u,k}^{\mathrm{MF}}\right|^2\right\}}{\left|\mathrm{DS}_{u,k}^{\mathrm{MF}}\right|^2} \\ &= \frac{\sum_{m=1}^{M}c_{mk}\left(2\tilde{\bar{\boldsymbol{h}}}_{mk}^H\boldsymbol{\Gamma}_{mk}\tilde{\bar{\boldsymbol{h}}}_{mk}+\mathrm{Tr}\left(\tilde{\boldsymbol{R}}_{mk}\boldsymbol{\Gamma}_{mk}\right)\right)}{\left(\sum_{m=1}^{M}c_{mk}\left(\tilde{\bar{\boldsymbol{h}}}_{mk}^H\tilde{\bar{\boldsymbol{h}}}_{mk}+\mathrm{Tr}(\boldsymbol{\Gamma}_{mk})\right)\right)^2}. \end{aligned} \tag{42}$$

Confronting (40) and (42), it is important to note that whereas in the DL segment the hardening ratio depends on the power allocation strategy, the UL scheme shows no power control dependency since a MS assigns the same power coefficient to the communication with every AP.

We now introduce particular cases to compare with our baseline spatially correlated Ricean fading model. For brevity of exposition, we drop the UL segment in subsequent analysis since calculations are roughly the same.

1) IMPACT OF LOS COMPONENT

For simplicity, let us consider an scenario with single-antenna APs, i.e. $\boldsymbol{R}_{mk}=\beta_{mk}\boldsymbol{I}_1$ and $\boldsymbol{\Gamma}_{mk}=\frac{1}{1+K_{mk}}\gamma_{mk}\boldsymbol{I}_1$ with

$$\gamma_{mk}=\frac{\tau_p\rho_p\beta_{mk}^2}{\tau_p\rho_p\sum_{k'=1}^{K}\beta_{mk'}\left|\boldsymbol{\varphi}_{k'}^H\boldsymbol{\varphi}_k\right|^2+1}. \tag{43}$$

If we further assume fully orthogonal and noiseless pilots ($\gamma_{mk}=\beta_{mk}$), we may rewrite (40) as

$$\begin{aligned}\xi_{d,k}^{\mathrm{CB}}\Big|_{\substack{\mathrm{LOS}\\\mathrm{CSI}}} &= \frac{\sum_{m=1}^{M}c_{mk}\eta_{mk}\left(2|\tilde{\bar{h}}_{mk}|^2\frac{\beta_{mk}}{K_{mk}+1}+\left(\frac{\beta_{mk}}{K_{mk}+1}\right)^2\right)}{\left(\sum_{m=1}^{M}c_{mk}\sqrt{\eta_{mk}}\left(|\tilde{\bar{h}}_{mk}|^2+\frac{\beta_{mk}}{K_{mk}+1}\right)\right)^2} \\ &= \frac{\sum_{m=1}^{M}c_{mk}\eta_{mk}\left(\frac{\beta_{mk}}{1+K_{mk}}\right)^2(2K_{mk}+1)}{\left(\sum_{m=1}^{M}c_{mk}\sqrt{\eta_{mk}}\beta_{mk}\right)^2}, \end{aligned} \tag{44}$$

where $\tilde{\bar{h}}_{mk}$ is the single-antenna case of (4) and $|\tilde{\bar{h}}_{mk}|^2=\frac{K_{mk}}{K_{mk}+1}\beta_{mk}$. Given the Ricean factor dependency of the numerator, it is easy to check that this ratio decreases as K_{mk} increases, and it is maximum when $K_{mk}=0$, i.e. NLOS scenarios. Note that the loss of orthogonality between noisy pilots and the fact of having multiple antennas at the APs do not alter the Ricean factor. These simplifications are assumed for the sake of exposition, but the insights given by (44) will hold regardless the initial considerations. This way, the following key observation is given.

Key observation: *The presence of a dominant LOS component in the wireless link between a given MS and the corresponding APs will always help the channel to harden, regardless the power coefficients and/or the particular clustering strategy.*

From an engineering perspective, one can guarantee a high probability of having a dominant LOS component by deploying APs at locations with good visibility. Moreover, deploying dense networks, such as CF massive MIMO and its derived approaches, would also assure LOS since the probability for a MS to be close to an AP is considerably high.

2) IMPACT OF SPATIAL CORRELATION

Without loss of generality, let us evaluate a multi-antenna APs scenario in which there is no dominant LOS component, i.e. $K_{mk} = 0 \ \forall mk$, leading to a correlated Rayleigh fading channel situation. Consequently, the terms $2\tilde{\tilde{\boldsymbol{h}}}_{mk}^{H}\boldsymbol{\Gamma}_{mk}\tilde{\tilde{\boldsymbol{h}}}_{mk}$ and $\tilde{\tilde{\boldsymbol{h}}}_{mk}^{H}\tilde{\tilde{\boldsymbol{h}}}_{mk}$ in both in the numerator and denominator of (40) vanish and $\tilde{\boldsymbol{R}}_{mk} = \boldsymbol{R}_{mk}$ resulting in

$$\xi_{d,k}^{\mathrm{CB}}\Big|_{\substack{\text{correlated}\\ \text{Rayleigh}}} = \frac{\sum_{m=1}^{M} c_{mk}\eta_{mk}\mathrm{Tr}\left(\boldsymbol{R}_{mk}\boldsymbol{\Gamma}_{mk}\right)}{\left(\sum_{m=1}^{M} c_{mk}\sqrt{\eta_{mk}}\mathrm{Tr}(\boldsymbol{\Gamma}_{mk})\right)^{2}}. \tag{45}$$

In addition, consider again perfect CSI and no pilot contamination ($\boldsymbol{R}_{mk} = \boldsymbol{\Gamma}_{mk}$) giving

$$\begin{aligned}\xi_{d,k}^{\mathrm{CB}}\Big|_{\substack{\text{correlated}\\ \text{Rayleigh}\\ \text{CSI}}} &= \frac{\sum_{m=1}^{M} c_{mk}\eta_{mk}\mathrm{Tr}\left(\boldsymbol{R}_{mk}^{2}\right)}{\left(\sum_{m=1}^{M} c_{mk}\sqrt{\eta_{mk}}\mathrm{Tr}\left(\boldsymbol{R}_{mk}\right)\right)^{2}}\\ &= \frac{\sum_{m=1}^{M} c_{mk}\eta_{mk}\beta_{mk}^{2}\mathrm{Tr}\left(\overline{\boldsymbol{R}}_{mk}^{2}\right)}{N^{2}\left(\sum_{m=1}^{M} c_{mk}\sqrt{\eta_{mk}}\beta_{mk}\right)^{2}},\end{aligned} \tag{46}$$

with $\overline{\boldsymbol{R}}_{mk} = \boldsymbol{R}_{mk}/\beta_{mk}$. In order to have some insights on the impact that spatial correlation may have on the hardening ratio, let us particularize (46) to an uncorrelated arrays situation ($\overline{\boldsymbol{R}}_{mk} = \boldsymbol{I}_N$), giving

$$\begin{aligned}\xi_{d,k}^{\mathrm{CB}}\Big|_{\substack{\text{uncorrelated}\\ \text{Rayleigh}\\ \text{CSI}}} &= \frac{\sum_{m=1}^{M} c_{mk}\eta_{mk}\beta_{mk}^{2}\mathrm{Tr}\left(\boldsymbol{I}_N\right)}{N^{2}\left(\sum_{m=1}^{M} c_{mk}\sqrt{\eta_{mk}}\beta_{mk}\right)^{2}}\\ &= \frac{\sum_{m=1}^{M} c_{mk}\eta_{mk}\beta_{mk}^{2}}{N\left(\sum_{m=1}^{M} c_{mk}\sqrt{\eta_{mk}}\beta_{mk}\right)^{2}}.\end{aligned} \tag{47}$$

Confronting (46) and (47), and owing to the fact that $\mathrm{Tr}\left(\overline{\boldsymbol{R}}_{mk}^{2}\right) \geq \mathrm{Tr}\left(\boldsymbol{I}_N\right) = N$ (with equality only for the uncorrelated case) since $\overline{\boldsymbol{R}}_{mk}$ is a positive semi-definite matrix (i.e. $\boldsymbol{r}^{H}\overline{\boldsymbol{R}}_{mk}\boldsymbol{r} \geq 0 \ \forall \boldsymbol{r} \in \mathbb{C}^{N\times 1}$), the hardening ratio in a spatially correlated scenario will always be higher than in the uncorrelated counterpart. The following key observation is given.

Key observation: *Under a multi-antenna APs scenario, the spatial correlation between the antennas conforming the array of a particular AP will imply a channel hardening degradation in comparison to the scenario with uncorrelated antennas.*

Though the massive MIMO channel has been shown to be spatially correlated in most situations, a particular scenario in which this may not happen implies equipping APs with half-wavelength spaced ULAs in a rich scattering location. It also worth mentioning that, in particular scenarios with large K, spatial correlation can indeed have a positive effect in reducing multi-user interference [15].

3) IMPACT OF UC APPROACHES

Regardless of any of the previous assumed scenarios, the hardening ratio will experience dependency on the connectivity coefficients. For simplicity, we take (47) as reference. The denominator grows faster than the numerator, so hardening will be enhanced when $c_{mk} = 1 \ \forall mk$, i.e. original CF scheme, while it will be degraded when employing any UC approach, as stated as follows.

Key observation: *Given the same network deployment with different clustering configurations, the pure CF scheme in which all APs provide service to all MSs will be the best case scenario in terms of channel hardening when compared to any other UC strategy.*

The impact of the clustering strategies will be most dependent on the APs density. As it will be shown later, for the traditional $D = 1000$ m deployment area, only a small fraction of the total of APs in the CF scheme will effectively contribute in terms of power to the channe hardening.

To sum up, it has been shown that the total number of antennas in the network is far from being the only factor affecting the channel hardening ratio. There are many other factors that needed to be taken into account when designing a CF massive MIMO network if one is to assure a certain hardening degree.

B. HARDENING RATIO WITH COOPERATIVE PROCESSING

We estimate now the hardening ratio for the case of ZF processing. Recalling (26) we may define $\mathrm{DS}_{d,k}^{\mathrm{ZF}} \triangleq \sqrt{\rho_d\omega_k}$ and

$$\begin{aligned}&\mathbb{E}\left\{\left|\mathrm{EN}_{d,k}\right|^{2}\right\}\\ &\quad= \mathbb{E}\left\{\left|\sqrt{\rho_d}\boldsymbol{\epsilon}_k^{T}\hat{\boldsymbol{G}}_c^{*}\left(\hat{\boldsymbol{G}}_c^{T}\hat{\boldsymbol{G}}_c^{*}\right)^{-1}\boldsymbol{\Omega}\boldsymbol{s}_d\right|^{2}\right\}\end{aligned}$$

$$= \rho_d \mathrm{Tr}\left(\boldsymbol{\Omega}^2 \mathbb{E}\left\{\left(\hat{\boldsymbol{G}}_c^T \hat{\boldsymbol{G}}_c^*\right)^{-1} \hat{\boldsymbol{G}}_c^T \tilde{\boldsymbol{A}}_k^* \hat{\boldsymbol{G}}_c^* \left(\hat{\boldsymbol{G}}_c^T \hat{\boldsymbol{G}}_c^*\right)^{-1}\right\}\right)$$
$$= \rho_d \mathrm{Tr}\left(\boldsymbol{\Omega}^2 \mathbb{E}\left\{\boldsymbol{W}^H \tilde{\boldsymbol{A}}_k^* \boldsymbol{W}\right\}\right)$$
$$= \rho_d \sum_{k'=1}^{K} \omega_{k'} \varrho_{kk'}, \tag{48}$$

with $\varrho_{kk'}$ being the k'-th entry in vector

$$\boldsymbol{\varrho}_k = \mathrm{diag}\left(\mathbb{E}\left\{\boldsymbol{W}^H \tilde{\boldsymbol{A}}_k^* \boldsymbol{W}\right\}\right), \tag{49}$$

and $\tilde{\boldsymbol{A}}_k = \mathcal{D}\left(\tilde{\boldsymbol{A}}_{1k}, \ldots, \tilde{\boldsymbol{A}}_{Mk}\right)$ with $\tilde{\boldsymbol{A}}_{mk} = c_{mk}\boldsymbol{A}_{mk}$. Note that $\boldsymbol{\varrho}_k$ represents the vector of interfering terms caused by the use of the channel estimates, rather than the true values, when designing the ZF matrix $\mathbf{W}$. As in [28], it is worth mentioning that the term $\mathbb{E}\left\{\left|\mathrm{EN}_{d,k}\right|^2\right\}$ cannot be computed in closed-form and must be estimated via Monte-Carlo simulation. At this point we may define $\mathrm{BU}_{d,k}^{\mathrm{ZF}} \triangleq \sqrt{\rho_d \omega_k \varrho_{kk}}$ leading to the DL channel hardening ratio with ZF precoding expressed as

$$\xi_{d,k}^{\mathrm{ZF}} = \frac{\mathbb{E}\left\{\left|\mathrm{BU}_{d,k}^{\mathrm{ZF}}\right|^2\right\}}{\left|\mathrm{DS}_{d,k}^{\mathrm{ZF}}\right|^2} = \frac{\left|\sqrt{\rho_d \omega_k \varrho_{kk}}\right|^2}{\rho_d \omega_k} = \varrho_{kk}. \tag{50}$$

Similar analysis follows for the UL segment. From (36) we define $\mathrm{DS}_{u,k}^{\mathrm{ZF}} \triangleq \sqrt{\rho_u \theta_k}$ and

$$\mathbb{E}\left\{\left|\mathrm{EN}_{u,k}\right|^2\right\} = \mathbb{E}\left\{\left|\sqrt{\rho_u \theta_k}\boldsymbol{w}_k^T \boldsymbol{\epsilon}_k s_{u,k}\right|^2\right\}$$
$$= \rho_u \mathrm{Tr}\left(\mathbb{E}\left\{\boldsymbol{E}^H \boldsymbol{w}_k^H \boldsymbol{w}_k \boldsymbol{E}\right\}\right)$$
$$= \rho_u \mathrm{Tr}\left(\theta_k \mathbb{E}\left\{\boldsymbol{W}^H \tilde{\boldsymbol{A}}_k \boldsymbol{W}\right\}\right)$$
$$= \rho_u \sum_{k'=1}^{K} \theta_{k'} \upsilon_{kk'}, \tag{51}$$

with $\upsilon_{kk'}$ being the k-th entry in vector.

$$\boldsymbol{\upsilon}_k = \mathrm{diag}\left(\mathbb{E}\left\{\boldsymbol{W}^H \tilde{\boldsymbol{A}}_k \boldsymbol{W}\right\}\right), \tag{52}$$

If we define $\mathrm{BU}_{u,k}^{\mathrm{ZF}} \triangleq \sqrt{\rho_u \theta_k \upsilon_{kk}}$, the UL channel hardening ratio with ZF combining is expressed as

$$\xi_{u,k}^{\mathrm{ZF}} = \frac{\mathbb{E}\left\{\left|\mathrm{BU}_{u,k}^{\mathrm{ZF}}\right|^2\right\}}{\left|\mathrm{DS}_{u,k}^{\mathrm{ZF}}\right|^2} = \frac{\left|\sqrt{\rho_u \theta_k \upsilon_{kk}}\right|^2}{\rho_u \theta_k} = \upsilon_{kk}. \tag{53}$$

As for (50), there is no closed-form expression for (53), so the possible impact that spatial correlation or the LOS component may have on the hardening under ZF, to the best of authors' knowledge, can only be deduced from simulation results. Nevertheless, we can point out that power control coefficients have no influence whatsoever on either DL or UL hardening with ZF processing.

VI. ACHIEVABLE RATES

The measured channel hardening ratio based on the joint propagation channel introduced in Section V directly affects the estimated DL/UL achievable rates since when hardening is compromised, these rates can underestimate the true performance of the network. It is important at this point to mention that critical optimization steps, such as the derivation of optimal power control coefficients (e.g. max-min) or the allocation of pilots, often rely on the closed-form achievable rate expressions, thus reinforcing the need for them to be as close as possible to the true system performance. Achievable DL/UL rates for single-antenna CF massive MIMO were first derived in [5] based on the classical massive MIMO literature leading to closed-form expressions valid for the CB/MF processing. Extending these expressions to the multi-antenna scenario leads to very straightforward computation (see, for instance, [6], [43]), while calculations when assuming spatial correlation or a LOS component can be found in the recent CF literature [17]–[24]. In this section we further develop the DL and UL achievable user rates previously given in the literature for the proposed spatially correlated Ricean fading channel model. Also, we propose user data rates benchmarks for comparison purposes which will give insight on the effects that a certain hardening degree may have on the achievable rate bounds.

Regardless of whether distributed or cooperative processing is conducted, the DL/UL use-and-then-forget bound of the achievable rate for the k-th MS (measured in bps) is defined as [5]

$$\mathcal{R}_{a,k}^{\mathrm{BF}} = \tilde{B}\log_2(1 + \mathrm{SINR}_{a,k}^{\mathrm{BF}}), \tag{54}$$

where

$$\tilde{B} = B\frac{1 - \tau_p/\tau_c}{2}, \tag{55}$$

with B denoting the system bandwidth and $\mathrm{BF} \in \{\mathrm{CB}, \mathrm{MF}, \mathrm{ZF}\}$. The term $1 - \tau_p/\tau_c$ represents the losses due to the training phase, while the factor $1/2$ accounts for the equal time-frequency split between UL and DL. The signal-to-interference-plus-noise ratio (SINR) will vary depending on the beamforming in use.

A. ACHIEVABLE RATES FOR DISTRIBUTED PROCESSING

Building on the work presented, for instance, in [3], [5], [44]–[46], the SINR can be derived as follows. In particular, the sum of the second, third and fourth terms in (20) are treated as *effective noise*. The additive terms constituting the *effective noise* are mutually uncorrelated, and uncorrelated with $s_{d,k}$. Therefore, both the desired signal and the so-called *effective noise* are uncorrelated. Same reasoning applies for the UL scheme described in Section IV.

Recalling the fact that uncorrelated Gaussian noise represents the worst case, under the distributed precoding scenario and assuming only statistical CSI is available at the MS [5],

we may express the DL segment SINR as

$$\mathrm{SINR}_{d,k}^{\mathrm{CB}} = \frac{\left|\mathrm{DS}_{d,k}^{\mathrm{CB}}\right|^2}{\mathbb{E}\left\{\left|\mathrm{BU}_{d,k}^{\mathrm{CB}}\right|^2\right\} + \sum_{k'\neq k}^{K}\mathbb{E}\left\{\left|\mathrm{UI}_{d,kk'}^{\mathrm{CB}}\right|^2\right\} + 1}. \tag{56}$$

An exact closed-form expression for (56) is given in (57), shown at the bottom of the page, where

$$\mathcal{T}_{1,mk} = \tilde{\tilde{\boldsymbol{h}}}_{mk}^{H}\tilde{\tilde{\boldsymbol{h}}}_{mk} + \mathrm{Tr}\left(\boldsymbol{\Gamma}_{mk}\right), \tag{58}$$

$$\mathcal{T}_{2,mk} = 2\tilde{\tilde{\boldsymbol{h}}}_{mk}^{H}\boldsymbol{\Gamma}_{mk}\tilde{\tilde{\boldsymbol{h}}}_{mk} + \mathrm{Tr}\left(\tilde{\boldsymbol{R}}_{mk}\boldsymbol{\Gamma}_{mk}\right), \tag{59}$$

$$\mathcal{T}_{3,mkk'} = \tilde{\tilde{\boldsymbol{h}}}_{mk}^{H}\boldsymbol{\Gamma}_{mk'}\tilde{\tilde{\boldsymbol{h}}}_{mk} + \left|\tilde{\tilde{\boldsymbol{h}}}_{mk}^{H}\tilde{\boldsymbol{R}}_{mk}^{1/2}\tilde{\tilde{\boldsymbol{h}}}_{mk'}\right|^2 + \tilde{\tilde{\boldsymbol{h}}}_{mk'}^{H}\tilde{\boldsymbol{R}}_{mk}\tilde{\tilde{\boldsymbol{h}}}_{mk'} + \mathrm{Tr}\left(\tilde{\boldsymbol{R}}_{mk}\boldsymbol{\Gamma}_{mk'}\right), \tag{60}$$

and

$$\mathcal{T}_{4,mkk'} = \tilde{\tilde{\boldsymbol{h}}}_{mk}^{H}\tilde{\tilde{\boldsymbol{h}}}_{mk'} + \left|\boldsymbol{\varphi}_{k'}^{H}\boldsymbol{\varphi}_{k}\right|^2 \mathrm{Tr}\left(\tilde{\boldsymbol{R}}_{mk}\boldsymbol{\Gamma}_{mk'}\tilde{\boldsymbol{R}}_{mk}^{-1}\right). \tag{61}$$

The computation of $\mathcal{T}_{1,mk}$ and $\mathcal{T}_{2,mk}$ is performed as denominator and numerator of (40), respectively, while the computation of $\mathcal{T}_{3,mk}$ and $\mathcal{T}_{4,mk}$ is again based on (41) and [5, Appendix A].

Following a similar procedure, and taking into account the collective noise term coming from all MSs, the UL segment SINR can be expressed as

$$\mathrm{SINR}_{u,k}^{\mathrm{MF}} = \frac{\left|\mathrm{DS}_{u,k}^{\mathrm{MF}}\right|^2}{\mathbb{E}\left\{\left|\mathrm{BU}_{u,k}^{\mathrm{MF}}\right|^2\right\} + \sum_{k'\neq k}^{K}\mathbb{E}\left\{\left|\mathrm{UI}_{u,kk'}^{\mathrm{MF}}\right|^2\right\} + \mathrm{NT}_{u,k}^{\mathrm{MF}}}. \tag{62}$$

An exact closed-form expression for (62) is given in (63), shown at the bottom of the page.

B. TRUE AND UPPER BOUND RATES

Since (54) in based on the worst case scenario, it is considered as a lower bound in terms of spectral efficiency, though the true network performance may be considerably better. Achieving a good channel hardening ratio translates into a large agreement between the achievable and true rates. In contrast, when hardening is compromised this true performance may be underestimated. A benchmark to compare the achievable rate with is the true network capacity under the assumption that the receiver only knows the statistical CSI. This is defined as

$$\mathcal{R}_{d,k}^{\mathrm{true}} = \tilde{B}\mathbb{E}\left\{\log_2\left(1 + \frac{\left|\mathrm{DS}_{d,k}^{\mathrm{CB}}\right|^2}{\left|\mathrm{BU}_{d,k}^{\mathrm{CB}}\right|^2 + \sum_{k'\neq k}^{K}\left|\mathrm{UI}_{d,kk'}^{\mathrm{CB}}\right|^2 + 1}\right)\right\}. \tag{64}$$

The gap between (54) and true rate reduces as the hardening ratio becomes smaller. It seems obvious that in order to achieve the maximum hardening possible the instantaneous channel gain must be equal to its mean when averaged through several small-scale fading realizations, i.e. $\left|\mathrm{BU}_{d,k}^{\mathrm{CB}}\right|^2 = 0$. The data rate that a genie-aided user that perfectly knows the instantaneous CSI is given by the upper bound achievable rate defined as

$$\mathcal{R}_{d,k}^{\mathrm{upper}} = \tilde{B}\mathbb{E}\left\{\log_2\left(1 + \frac{\rho_d\sum_{M=1}^{M}\left|\boldsymbol{\varpi}_{d,mk}\boldsymbol{g}_{mk}\right|^2}{\sum_{k'\neq k}^{K}\left|\mathrm{UI}_{d,kk'}^{\mathrm{CB}}\right|^2 + 1}\right)\right\}, \tag{65}$$

which indeed represents the maximum channel capacity. Though these latter expressions are specifically intended for the DL segment, conclusions are also valid for the UL since in both cases the decoding entity, i.e. the MS or the CPU, relies on statistical CSI.

$$\mathrm{SINR}_{d,k}^{\mathrm{CB}} = \frac{\rho_d\left(\sum_{m=1}^{M}c_{mk}\sqrt{\eta_{mk}}\mathcal{T}_{1,mk}\right)^2}{\rho_d\sum_{m=1}^{M}c_{mk}\eta_{mk}\mathcal{T}_{2,mk} + \rho_d\sum_{k'\neq k}^{K}\left(\sum_{m=1}^{M}c_{mk'}\eta_{mk'}\mathcal{T}_{3,mkk'} + \left|\sum_{m=1}^{M}c_{mk'}\sqrt{\eta_{mk'}}\mathcal{T}_{4,mkk'}\right|^2\right) + 1} \tag{57}$$

$$\mathrm{SINR}_{u,k}^{\mathrm{MF}} = \frac{\rho_d\eta_k\left(\sum_{m=1}^{M}c_{mk}\mathcal{T}_{1,mk}\right)^2}{\rho_d\eta_k\sum_{m=1}^{M}c_{mk}\mathcal{T}_{2,mk} + \rho_d\sum_{k'\neq k}^{K}\eta_{k'}\left(\sum_{m=1}^{M}c_{mk'}\mathcal{T}_{3,mkk'} + \left|\sum_{m=1}^{M}c_{mk'}\mathcal{T}_{4,mkk'}\right|^2\right) + \sum_{m=1}^{M}c_{mk}\mathcal{T}_{1,mk}} \tag{63}$$

C. ACHIEVABLE RATES FOR COOPERATIVE PROCESSING

The diagonalizing structure of the ZF precoder allows the DL SINR for user k to be expressed as [28]

$$\mathrm{SINR}_{d,k}^{\mathrm{ZF}} = \frac{\left|\mathrm{DS}_{d,k}^{\mathrm{ZF}}\right|^2}{\mathbb{E}\left\{\left|\mathrm{BU}_{d,k}^{\mathrm{ZF}}\right|^2\right\} + \sum_{k'\neq k}^{K}\mathbb{E}\left\{\left|\mathrm{UI}_{d,kk'}^{\mathrm{ZF}}\right|^2\right\} + 1} = \frac{\left|\mathrm{DS}_{d,k}^{\mathrm{ZF}}\right|^2}{\mathbb{E}\left\{\left|\mathrm{EN}_{d,k}\right|^2\right\} + 1} = \frac{\rho_d \omega_k}{\rho_d \sum_{k'=1}^{K} \omega_{k'} \varrho_{kk'} + 1}, \tag{66}$$

where we have defined $\mathrm{UI}_{d,kk'}^{\mathrm{ZF}} \triangleq \sqrt{\rho_d \omega_{k'} \varrho_{kk'}}$ for $k' \neq k$. As in the hardening ratio, the denominator of (66) can only be estimated by Monte-Carlo simulation.

For the UL segment, we may express the SINR as

$$\mathrm{SINR}_{u,k}^{\mathrm{ZF}} = \frac{\left|\mathrm{DS}_{u,k}^{\mathrm{ZF}}\right|^2}{\mathbb{E}\left\{\left|\mathrm{BU}_{u,k}^{\mathrm{ZF}}\right|^2\right\} + \sum_{k'\neq k}^{K}\mathbb{E}\left\{\left|\mathrm{UI}_{u,kk'}^{\mathrm{ZF}}\right|^2\right\} + \mathrm{NT}_{u,k}^{\mathrm{ZF}}} = \frac{\left|\mathrm{DS}_{u,k}^{\mathrm{ZF}}\right|^2}{\mathbb{E}\left\{\left|\mathrm{EN}_{u,k}\right|^2\right\} + \mathrm{NT}_{u,k}^{\mathrm{ZF}}} = \frac{\rho_u \theta_k}{\rho_u \sum_{k'=1}^{K} \theta_{k'} \upsilon_{kk'} + \nu_k}, \tag{67}$$

where we have defined $\mathrm{UI}_{u,kk'}^{\mathrm{ZF}} \triangleq \sqrt{\rho_u \theta_{k'} \upsilon_{kk'}}$ for $k' \neq k$ and $\mathrm{NT}_{u,k}^{\mathrm{ZF}} \triangleq \nu_k$ as the k-th entry in vector $\mathrm{diag}\left(\mathbb{E}\left\{\boldsymbol{W}\boldsymbol{W}^H\right\}\right)$. Again, there is no closed-form expression for the UL SINR.

True and upper rates can be computed via Monte-Carlo using analogous expressions to (64) and (65).

VII. POWER CONTROL STRATEGIES

Depending on whether the DL or UL segment is addressed and, particularly, on the processing scheme, power control strategies may have certain impact on the channel hardening. We have shown that ZF precoding and combining is totally agnostic of the power allocation since power coefficients are only MS-dependent. Same situation occurs on the UL segment with MF combining. Nevertheless, the hardening ratio is sensitive to power control under CB precoding. Each power control strategy here described is specifically designed for each precoder/combiner scheme, however, note that no matter the processing strategy, the power constraint (18) must be fulfilled. Every power control strategy used in this work is executed on a large-scale fading basis, i.e. power control coefficients need to be computed once every several coherence intervals.

A. DISTRIBUTED PROCESSING POWER CONTROL

Since power control influences the channel hardening ratio for the distributed processing DL segment, we employ two different power control approaches for comparison purposes: a low complexity heuristic uniform power allocation strategy and a max-min SINR optimal approach [5], [28].

1) DL UNIFORM POWER ALLOCATION

Under the uniform power allocation scheme an AP assigns the same power coefficient to every user. This power control scheme has negligible complexity, while it does not lose too much performance in terms of average user data rate if compared with the max-min SINR optimal solution [28]. Power coefficients for the DL segment are computed as follows. From (18) we have

$$\begin{aligned}
&\mathbb{E}\left\{\left\|\boldsymbol{x}_m^{\mathrm{CB}}\right\|^2\right\} \\
&= \rho_d \mathbb{E}\left\{\left|\boldsymbol{\varpi}_{d,k}\boldsymbol{g}_k\right|^2\right\} \\
&= \rho_d \mathbb{E}\left\{\left|\sum_{k=1}^{K} c_{mk}\eta_{mk}\hat{\boldsymbol{g}}_{mk}^H \boldsymbol{g}_{mk}\right|^2\right\} \\
&= \rho_d \sum_{k=1}^{K} c_{mk}\eta_{mk}\mathbb{E}\left\{\left\|\hat{\boldsymbol{g}}_{mk}\right\|^2\right\} \\
&= \rho_d \sum_{k=1}^{K} c_{mk}\eta_{mk}\left(\frac{K_{mk}}{K_{mk}+1}N\beta_{mk} + \mathrm{Tr}\left(\boldsymbol{\Gamma}_{mk}\right)\right) \leq \rho_d,
\end{aligned} \tag{68}$$

which leads to

$$\eta_{mk} = \eta_m = \frac{1}{\sum_{k=1}^{K} c_{mk}\left(\frac{K_{mk}}{K_{mk}+1}N\beta_{mk} + \mathrm{Tr}\left(\boldsymbol{\Gamma}_{mk}\right)\right)}. \tag{69}$$

Note that whereas the UL power control coefficients are restricted to $0 \leq \eta_k \leq 1$, in the DL segment there is no restriction for η_{mk}, except for being positive. This computation can be performed locally at each AP, so there is no need to use the fronthaul link connection to the CPU for this particular purpose. This is a key aspect if fronthaul links are not supposed to have infinite capacity, which will be the case in practical scenarios.

2) DL MAX-MIN POWER ALLOCATION

The max-min power allocation schemes developed in [5], [28] ensure that the minimum SINR is maximized for every user. In particular scenarios where a large number of users is present, this strategy will lead to a performance reduction of the overall network due to particular MSs with bad channel conditions, however, it provides a more uniform service. The main drawback in this case is the considerable high computational overhead, which may result on making this power control scheme unfeasible in practical scenarios, while being mandatory to be performed at the CPU. Defining $\boldsymbol{\eta} = \left[\boldsymbol{\eta}_1^T, \ldots, \boldsymbol{\eta}_M^T\right]^T$ and $\boldsymbol{\eta}_m = [\eta_{m1}, \ldots, \eta_{mK}]^T$, the optimization problem is stated as

$$\begin{aligned}
&\max_{\boldsymbol{\eta}} \min_{k} \mathrm{SINR}_{d,k}^{\mathrm{CB}}, \\
&\text{s.t. } \left\|\boldsymbol{x}_m^{\mathrm{CB}}\right\|^2 \leq \rho_d \ \forall m.
\end{aligned} \tag{70}$$

with $\boldsymbol{x}_m^{\mathrm{CB}}$ the m-th entry of (25). Using (57), (70) can be reformulated as

$$\max_{\boldsymbol{\varsigma},\boldsymbol{\lambda}} \min_{k} \frac{\left(\sum_{m=1}^{M} \varsigma_{mk} \mathcal{T}_{1,mk}\right)^2}{\sum_{m=1}^{M}\sum_{k'=1}^{K} \varsigma_{mk'}^2 \varkappa_{mkk'} + \sum_{k'\neq k}^{K} |\lambda_{kk'}|^2 + \frac{1}{\rho_d}},$$
$$\text{s.t.} \sum_{m=1}^{M} \varsigma_{mk'} \mathcal{T}_{4,mkk'} \leq \lambda_{kk'} \ \forall k' \neq k,$$
$$\sum_{k'=1}^{K} \varsigma_{mk'}^2 \mathbb{E}\left\{ \left\| \boldsymbol{\varpi}_{d,mk'} \right\|^2 \right\} \leq 1 \ \forall m,$$
$$\varsigma_{mk} \geq 0 \ \forall mk, \tag{71}$$

where we have introduced the slack variables $\lambda_{kk'}$ and have used the definitions $\varsigma_{mk} = \sqrt{\eta_{mk}}$ and

$$\varkappa_{mkk'} = \begin{cases} \mathcal{T}_{2,mk}, & k' = k \\ \mathcal{T}_{3,mkk'}, & k' \neq k. \end{cases} \tag{72}$$

Problem (71) is a quasi-concave optimization problem that can be expressed in an equivalent form as

$$\max_{\boldsymbol{\varsigma},\boldsymbol{\lambda},x} x$$
$$\text{s.t.} \sqrt{x} \left\| \boldsymbol{\vartheta}_{1k}, \ldots, \boldsymbol{\vartheta}_{Mk} \bar{\boldsymbol{\lambda}}_k \frac{1}{\sqrt{\rho_d}} \right\|_F \leq \sum_{m=1}^{M} \varsigma_{mk} \mathcal{T}_{1,mk} \ \forall k,$$
$$\sum_{m=1}^{M} \varsigma_{mk'} \mathcal{T}_{4,mkk'} \leq \lambda_{kk'} \ \forall k' \neq k,$$
$$\sum_{k'=1}^{K} \varsigma_{mk'}^2 \mathbb{E}\left\{ \left\| \boldsymbol{\varpi}_{d,mk'} \right\|^2 \right\} \leq 1 \ \forall m,$$
$$\varsigma_{mk} \geq 0 \ \forall mk, \tag{73}$$

where $\boldsymbol{\vartheta}_{mk} = \left[\varsigma_{m1}\sqrt{\varkappa_{mk1}}, \ldots, \varsigma_{mK}\sqrt{\varkappa_{mkK}}\right]$ and $\boldsymbol{\lambda}_k = \left[\lambda_{k1}, \ldots, \lambda_{k(k-1)}, \lambda_{k(k+1)}, \ldots, \lambda_{kK}\right]$. Problem (73) is a second order cone (SOC) program that can be efficiently solved by using a conventional iterative bisection search algorithm. Specific details on the optimality, complexity and feasibility of these algorithms were fully commented by Ngo *et al.* in the seminal paper [5].

3) UL FULL POWER ALLOCATION

Though there are several proposals for UL power control in the literature, we are assuming full power transmission, i.e. $\eta_k = 1$, since it has been shown to work rather well, even outmatching the max-min SINR optimal approach in terms of average sum-rate, as shown in [21] and [47].

B. COOPERATIVE PROCESSING POWER CONTROL

1) DL LOW-COMPLEXITY MAX-MIN POWER ALLOCATION

As in the distributed precoding power allocation scenario, finding the optimal DL power coefficients that satisfy the max-min SINR criteria for cooperative precoding involves solving a similar optimization problem (though with less complexity since only K coefficients need to be computed), stated as

$$\max_{\omega_1,\ldots,\omega_K} \min \mathrm{SINR}_{d,k}^{\mathrm{ZF}}$$
$$\text{s.t.} \left\| \boldsymbol{x}_m^{\mathrm{ZF}} \right\|^2 \leq \rho_d \ \forall m, \tag{74}$$

where the transmitted power from the m-th AP is

$$\begin{aligned} \left\| \boldsymbol{x}_m^{\mathrm{ZF}} \right\|^2 &= \rho_d \mathbb{E}\left\{ \boldsymbol{w}_m^T \boldsymbol{w}_m^* \right\} \\ &= \rho_d \mathbb{E}\left\{ \left(\hat{\boldsymbol{g}}_{c,m}^H \left(\hat{\boldsymbol{G}}_c^T \hat{\boldsymbol{G}}_c^* \right) \boldsymbol{\Omega} \right) \left(\hat{\boldsymbol{g}}_{c,m}^H \left(\hat{\boldsymbol{G}}_c^T \hat{\boldsymbol{G}}_c^* \right) \boldsymbol{\Omega} \right)^H \right\} \\ &= \rho_d \mathrm{Tr}\left(\boldsymbol{\Omega}^2 \mathbb{E}\left\{ \left(\hat{\boldsymbol{G}}_c^T \hat{\boldsymbol{G}}_c^* \right)^{-1} \hat{\boldsymbol{g}}_{c,m}^T \hat{\boldsymbol{g}}_{c,m}^* \left(\hat{\boldsymbol{G}}_c^T \hat{\boldsymbol{G}}_c^* \right)^{-1} \right\} \right) \\ &= \rho_d \sum_{k'=1}^{K} \omega_{k'} \delta_{kk'}, \end{aligned} \tag{75}$$

being $\boldsymbol{w}_m$ is the row vector of matrix $\boldsymbol{W}$ and $\delta_{kk'}$ the k'-th entry of

$$\boldsymbol{\delta}_m = \mathrm{diag}\left(\mathbb{E}\left\{ \left(\hat{\boldsymbol{G}}_c^T \hat{\boldsymbol{G}}_c^* \right)^{-1} \hat{\boldsymbol{g}}_{c,m}^T \hat{\boldsymbol{g}}_{c,m}^* \left(\hat{\boldsymbol{G}}_c^T \hat{\boldsymbol{G}}_c^* \right)^{-1} \right\} \right). \tag{76}$$

Note that power coefficients will differ only between users as a necessity for canceling the interference between MSs. The solution of (74) relies as well on the bisection method and has less online overhead as it would have in the distributed processing scenario since the power coefficient for the k-th MS will be the same regardless the AP. In the particular case of having an error-free estimation, problem (74) can be solved through a heuristic and low complexity approach having the power coefficient computed as [28]

$$\omega_1 = \ldots = \omega_K = 1 / \left(\max_m \sum_{k=1}^{K} \delta_{mk} \right). \tag{77}$$

Channel estimation in this work is nevertheless imperfect and the solution obtained with this low complexity approach will differ from the optimal one. However, as shown in [28], this approach nearly matches the optimal max-min SINR solution while considerably reducing the computational overhead at the CPU making it suitable for real deployments.

2) UL FULL POWER ALLOCATION

As in the distributed scenario, we use a full power allocation strategy for the UL segment under the cooperative combining scheme, i.e. $\theta_k = 1$.

VIII. NUMERICAL RESULTS

The baseline scenario for the simulations will consist of a uniform distribution of APs and MSs on a square coverage area with side D. This setup is roughly similar to those presented in previous work on CF massive MIMO, such as [4], [5], [8], [29], among others. In order to avoid boundary effects, a wrapped-around technique is implemented at the edges of coverage area making the results virtually equivalent to those

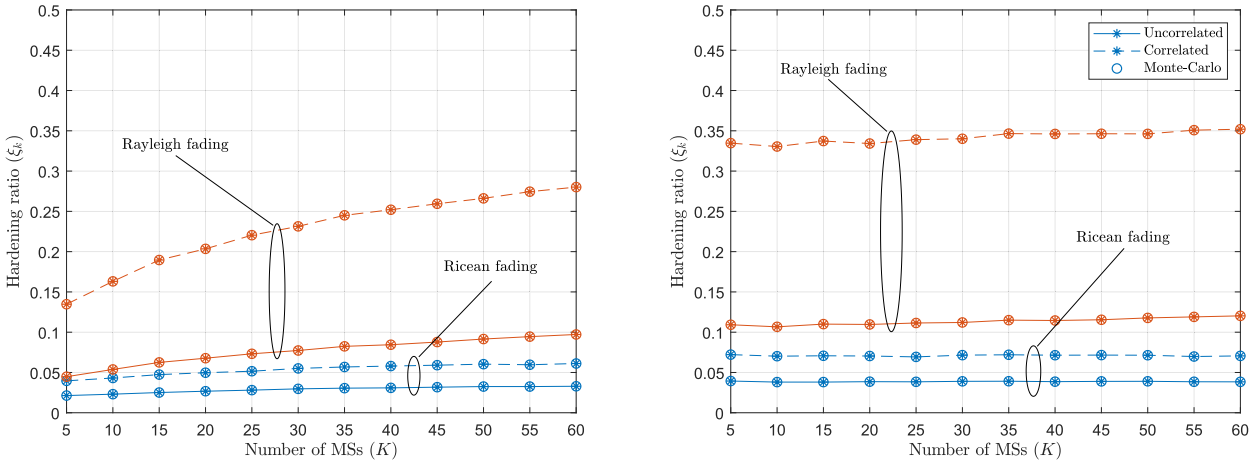

(a) DL (b) UL

FIGURE 1. Channel hardening ratio for CF with CB precoding and MF combining using uniform power allocation having each AP $N = 4$.

TABLE 1. Simulation default parameters.

Parameter	Value
Carrier frequency (f_0)	2 GHz
System bandwidth (B)	20 MHz
Side of square coverage area (D)	1000 m
Number of APs (M)	100
Noise figure at AP and MS (NF)	9 dB
Available average power at the AP (P_d)	200 mW
Available average power at the MS (P_u)	100 mW
AP antenna height (h_{AP})	15 m
MS antenna height, h_{MS})	1.65 m
Channel coherence interval length (τ_c)	200 samples
Training phase interval length (τ_p)	20 samples
Payload phase interval length ($\tau_d = \tau_u$)	$(\tau_c - \tau_p)/2$ samples
LOS reference distance (d_0)	20 m
Path loss parameters (L_0, α, σ_χ)	
- LOS, $d_{mk} \leq 150$ m	34, 2.2, 3 dB
- LOS, $d_{mk} > 150$ m	-5.17, 4, 3 dB
- NLOS	30, 3.67, 4 dB
Shadow fading decorrelation distance	9 m
Shadow fading correlation among APs	0.5
Ricean K-factor distribution (μ_K, σ_K)	9 dB, 5 dB
Distribution of the AoA deviation	$\mathcal{N} \sim (0, \sigma_\zeta^2)$
ASD	10

achieved in an infinite network. All simulation parameters will remain as in Table 1, unless stated otherwise in particular simulations.

We first show the channel hardening ratio under the pure CF scheme in Figs. 1a and 1b for both the DL and the UL segments, respectively. These results correspond to the CB/MF with the uniform power allocation strategy and $N = 4$. For comparison purposes, four different channel types are shown (uncorrelated Rayleigh fading, spatially correlated Rayleigh fading, uncorrelated Ricean fading and spatially correlated Ricean fading). To begin with, we point out the exact matching between the analytical and Monte-Carlo values for every case, thus confirming the accuracy of the hardening theoretical closed-form expressions for any scenario. While the UL is totally independent of the power coefficients as the hardening remains quasi-constant when varying K, this is not the case in the DL segment. This latter case shows a lower hardening ratio regardless the configuration when there are less active MSs owing to the fact that the same amount of power needs to be shared among less users. When comparing the Rayleigh and Ricean fading, it is clear that the existence of a strong LOS component is always beneficial and boosts channel hardening in either segment. Bear in mind that Ricean fading channels are often considered to be quasi-deterministic channels. This fact agrees with both Figs. 1a and 1b. In contrast, spatial correlation degrades the ratio, specially under Rayleigh fading.

Linking with Figs. 1, in Figs. 2a and 2b the achievable rates are presented for the same configurations. Again, a good matching is shown between Monte-Carlo simulations and the analytical closed-form expression values for any of the scenarios presented. Similarly to the hardening ratios, the LOS component of any of the two Ricean fading scenarios has significant impact on the system performance, while the correlation between AP antennas degrades it. It is worth mentioning that, as K grows, the spatial correlation enhances performance due to multi-user interference removal, thus reducing the gap between the correlated and uncorrelated curves. Anyhow, drawing conclusions of a CF massive MIMO network under the widely used uncorrelated Rayleigh fading channel model could be most misleading, as noted with the hardening ratios.

In Fig. 3 the CDF of the DL hardening ratio with CB precoding is shown for a set of $K = 10$ MSs, under uniform power allocation and max-min power allocation in Figs. 3a and 3b, respectively. Fig. 3a confirms what could already be seen in Fig. 1a; hardening is considerably degraded under spatially correlated Rayleigh fading implying a major gap to the uncorrelated Rayleigh scenario. Again, minor

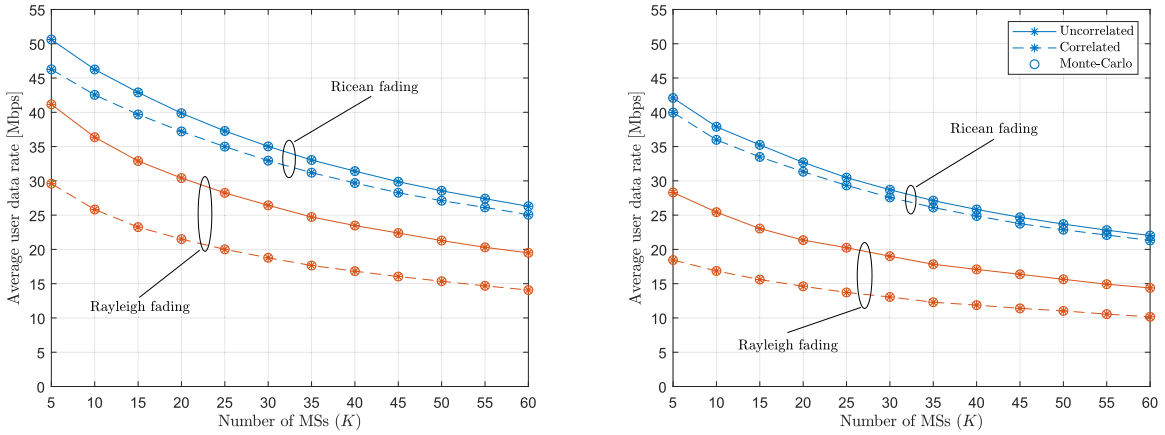

(a) DL (b) UL

FIGURE 2. Achievable rate for CF with CB precoding and MF combining using uniform power allocation having each AP $N = 4$.

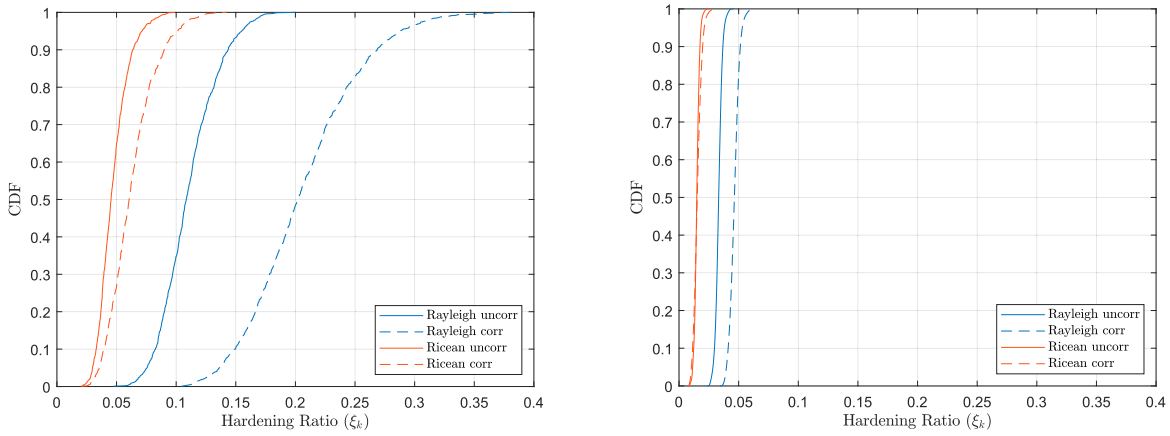

(a) Uniform Power Allocation (b) Max-Min Power Allocation

FIGURE 3. CDF of the DL hardening ratio with CB precoding having each AP $N = 2$ and $K = 10$.

differences are observed under the spatially correlated and uncorrelated Ricean fading scenarios. As for the max-min power control, a much steeper CDF is shown, owing to the fact of ensuring that every MS will experience the same SINR irrespective of its location in the coverage area. In contrast to the uniform power allocation, the max-min power control satisfies stronger hardening while the differences between the correlated and uncorrelated scenarios are considerably smaller, specially under Ricean fading.

Regarding cooperative processing, Fig. 4 shows the DL achievable rate with ZF precoding and the low-complexity max-min power control. As in Fig. 2a, we are showing all four channel configurations, i.e. Ricean/Rayleigh fading with spatially correlated/uncorrelated antennas. A good matching is shown between the proposed semi-analytical expressions and the pure Monte-Carlo simulations. Bear in mind that analytical expressions presented in this paper need Monte-Carlo computation. Similar to the distributed processing scenarios, the LOS component boosts the achievable rates. In contrast, under ZF precoding user date rate exhibits a slight enhancement for spatially correlated scenarios.

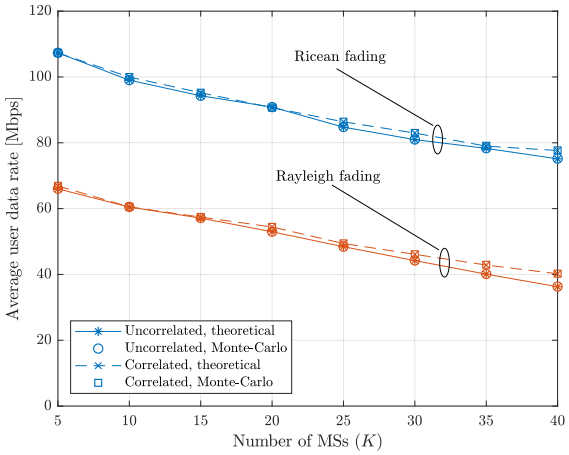

FIGURE 4. DL achievable rate with ZF precoding and low-complexity max-min power allocation having each AP $N = 2$.

In Fig. 5 the DL hardening ratio is shown for the different UC configurations and various coverage area sizes under a Rayleigh fading channel and $N = 1$. Note that

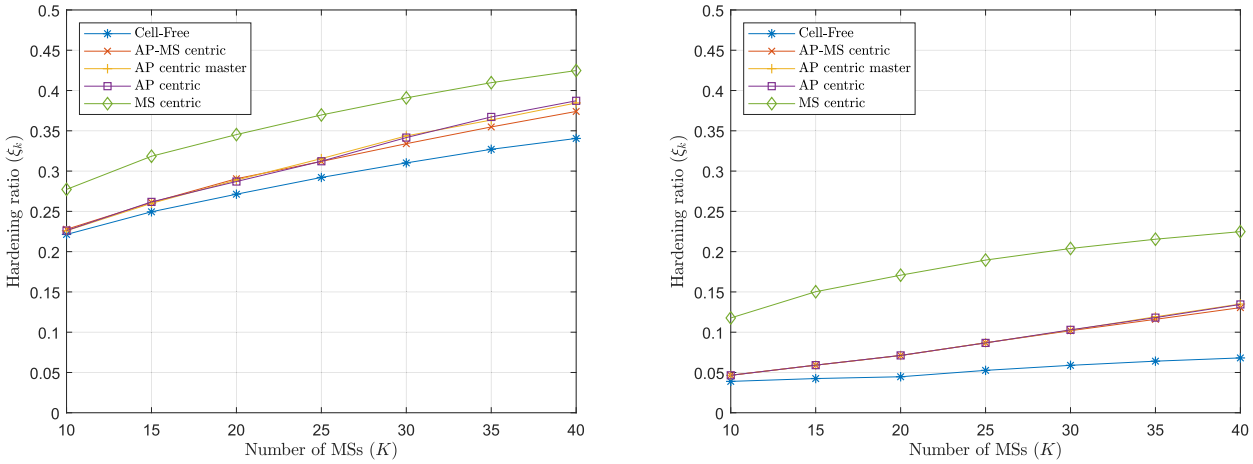

(a) $D = 1000$ m (b) $D = 100$ m

FIGURE 5. DL channel hardening with CB precoding using uniform power allocation for single-antenna APs ($N = 1$) under difference clustering strategies ($K_{UC} = M_{UC} = 5$).

TABLE 2. Average number of APs serving a MS and average number of MSs being served by an AP under different clustering strategies ($M = 100$ and $K_{UC} = M_{UC} = 5$).

	$K = 20$		$K = 60$	
Clustering scheme	**APs serving a MS**	**MSs served by an AP**	**APs serving a MS**	**MSs served by an AP**
CF	100	20	100	60
AP Centric	25	5	8.3333	5
AP Centric with Master AP	25.001	5.0002	8.3609	5.0165
MS Centric	7.2687	1.4538	5.2622	3.1573
AP-MS Centric	25.1015	5.0203	9.2132	5.528

conclusions drawn in this case do not vary no matter the fading type or having single or multi-antenna APs. CB precoding and uniform power allocation is considered. The classical CF scheme is shown for comparison purposes. Let us comment on every configuration, except for MS centric by now. Under the traditional $D = 1000$ m deployment area (Fig. 5a), there are little differences between all architectures. With the classical CF configuration, the number of APs effectively contributing to the hardening ratio tends to match the number of active APs in any of the UC configurations. In other words, the pure CF and the UC architectures perform similarly with minor differences. However, if K grows large enough, a particular MS will be served by less APs as their service needs to be split among more users. The gap between the UC schemes is highly conditioned by the AP deployment density, which is strictly related to the size of the coverage area. As for the MS centric scenario, since the number of APs serving a given MS remains static, the gap with the pure CF scheme will be the same regardless of the number of active users in the network. To sum up, the channel hardening ratio that a given MS experiences will be inversely proportional to the number APs providing service to that user. In Table 2 the average number of APs serving a MS and the average number of MSs being served by an AP under different clustering strategies are shown. It can be clearly seen that the MS centric strategy has the least number of APs serving a particular MS (thus having the worst channel hardening ratio in accordance to the third key observation in Section V). There are little differences between the rest of the schemes in accordance to what is shown on Fig. 5a. Now, turning our attention to Fig. 5b, the gap between CF and UC approaches slightly increases as more APs are effectively contributing in terms of hardening in the classical scheme. It is worth mentioning that, except for the MS centric architectures, all UC schemes perform equally in terms of hardening since the selection of APs from a given MS, and vice-versa, tends to be the same. Though a good degree of channel hardening is achieved, user data rate could be severely degraded due to strong pilot contamination when the coverage area is small.

The impact that spatial correlation has on the channel hardening ratio as a function of the number of APs is shown in Fig. 6. The hardening ratio for different values of the ASD plus an uncorrelated case for comparison is shown. Note that having 10° of ASD corresponds to strong correlation among antennas, while 40° implies a moderate correlation. As expected, hardening improves considerably as M grows large enough. Under Ricean fading, spatial correlation has a minor impact on the hardening, even if antennas are strongly correlated. However, when turning the attention to Rayleigh fading, the difference between an uncorrelated scenario and strong correlation is substantial. This confirms that assuming uncorrelated Rayleigh fading channel in CF massive MIMO

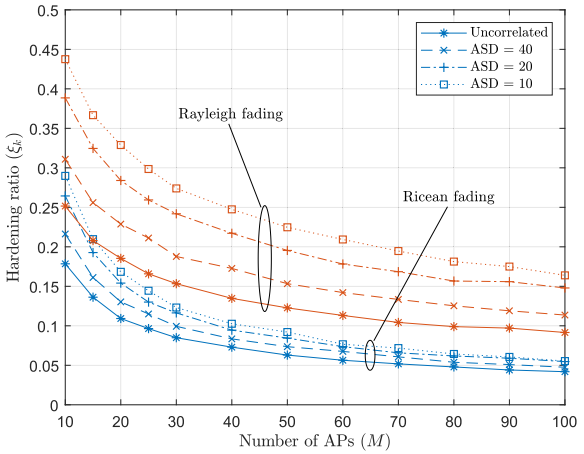

FIGURE 6. DL channel hardening ratio with CB precoding and uniform power allocation under Rayleigh fading having each AP $N = 2$.

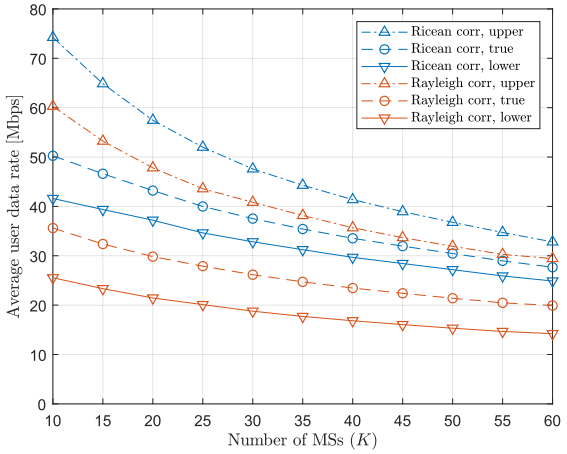

FIGURE 7. Average DL achievable rate with true and upper bounds under CB precoding and uniform power allocation having each AP $N = 4$.

networks with multi-antenna APs could lead to misleading conclusions.

Lastly, in Fig. 7 a comparison between the lower bound achievable rate, the true rate achieved in the absence of receiver CSI and upper bounds is shown. Focusing on the Rayleigh fading scenario, a remarkably large gap is observed between the achievable rate (which is always a lower bound in terms of performance) and the true network performance. This gap is strictly conditioned by the hardening ratio. A greater gap exists indeed if compared with the upper bound, which corresponds to the maximum channel capacity. If we now turn our attention to the Ricean fading scenario, where hardening is boosted thanks to the LOS component, the gap between bounds is reduced. These results prove that, even having multi-antenna APs, hardening is severely compromised in correlated Rayleigh scenarios and the true network performance is underestimated when relying on the closed-form achievable rates.

IX. CONCLUSION

In this work CF and UC massive MIMO networks under a spatially correlated Ricean fading channel have been analyzed under different precoding and combining strategies. Results show how the dominant LOS component of the Ricean fading has a positive impact both on the hardening ratio and user date rates. On the contrary, spatially correlated antenna arrays imply a channel hardening degradation for distributed processing schemes. Interestingly, if a cooperative ZF processing is considered, spatial correlation entails an enhancement in terms of user date rate over the uncorrelated scenario when the number of users in the network is considerably large. It has been also shown how the newly proposed UC based approaches imply a slight degradation of the channel hardening under the traditional deployment area of 1000×1000 m, but this degradation may considerably worsen if the coverage area is small. The widely used uncorrelated Rayleigh fading channel model overestimates the system performance in terms of both hardening and user rate. If one assumes a more realistic scenario in which antennas from each AP are spatially correlated, channel hardening is compromised and the commonly used achievable rate may underestimate the true system performance. In general, it has been shown that, even in scenarios with multi-antenna APs, one cannot take for granted channel hardening in CF massive MIMO networks, since it has a strong dependency on the channel characteristics, power control coefficients, clustering strategies and spatial density of APs. In this context, we have shown the existence of a gap between the true system performance and the estimated achievable rates in accordance with the degree of channel hardening that is achieved. Closed-form expressions for both the channel hardening ratio and the achievable user rate were derived for CB precoding and MF combining, while semi-analytical expressions were given for ZF. These analytical expressions can be used to perform the design and optimization of key aspects in CF massive MIMO networks, such as scheduling algorithms or clustering strategies, though this is left for future work.

REFERENCES

[1] R. Irmer, H. Droste, P. Marsch, M. Grieger, G. Fettweis, S. Brueck, H.-P. Mayer, L. Thiele, and V. Jungnickel, "Coordinated multipoint: Concepts, performance, and field trial results," *IEEE Commun. Mag.*, vol. 49, no. 2, pp. 102–111, Feb. 2011.

[2] D. Lee, H. Seo, B. Clerckx, E. Hardouin, D. Mazzarese, S. Nagata, and K. Sayana, "Coordinated multipoint transmission and reception in LTE-advanced: Deployment scenarios and operational challenges," *IEEE Commun. Mag.*, vol. 50, no. 2, pp. 148–155, Feb. 2012.

[3] T. L. Marzetta, E. G. Larsson, H. Yang, and H. Q. Ngo, *Fundamentals Massive MIMO*. Cambridge, U.K.: Cambridge Univ. Press, 2016.

[4] H. Q. Ngo, A. Ashikhmin, H. Yang, E. G. Larsson, and T. L. Marzetta, "Cell-free massive MIMO: Uniformly great service for everyone," in *Proc. IEEE 16th Int. Workshop Signal Process. Adv. Wireless Commun. (SPAWC)*, Jun. 2015, pp. 201–205.

[5] H. Q. Ngo, A. Ashikhmin, H. Yang, E. G. Larsson, and T. L. Marzetta, "Cell-free massive MIMO versus small cells," *IEEE Trans. Wireless Commun.*, vol. 16, no. 3, pp. 1834–1850, Mar. 2017.

[6] A. A. I. Ibrahim, A. Ashikhmin, T. L. Marzetta, and D. J. Love, "Cell-free massive MIMO systems utilizing multi-antenna access points," in *Proc. 51st Asilomar Conf. Signals, Syst., Comput.*, Oct. 2017, pp. 1517–1521.
[7] T. C. Mai, H. Quoc Ngo, and T. Q. Duong, "Cell-free massive MIMO systems with multi-antenna users," in *Proc. IEEE Global Conf. Signal Inf. Process. (GlobalSIP)*, Nov. 2018, pp. 828–832.
[8] S. Buzzi and C. D'Andrea, "Cell-free massive MIMO: User-centric approach," *IEEE Wireless Commun. Lett.*, vol. 6, no. 6, pp. 706–709, Dec. 2017.
[9] D. Gesbert, M. Kountouris, R. W. Heath, C.-B. Chae, and T. Salzer, "Shifting the MIMO paradigm," *IEEE Signal Process. Mag.*, vol. 24, no. 5, pp. 36–46, Sep. 2007.
[10] D. Dardari, "Channel hardening, favorable equalization and propagation in wideband massive MIMO," in *Proc. 27th Eur. Signal Process. Conf. (EUSIPCO)*, Sep. 2019, pp. 1–5.
[11] J. Zhang, S. Chen, Y. Lin, J. Zheng, B. Ai, and L. Hanzo, "Cell-free massive MIMO: A new next-generation paradigm," *IEEE Access*, vol. 7, pp. 99878–99888, 2019.
[12] G. Interdonato, H. Q. Ngo, E. G. Larsson, and P. Frenger, "How much do downlink pilots improve cell-free massive MIMO?" in *Proc. IEEE Global Commun. Conf. (GLOBECOM)*, Dec. 2016, pp. 1–7.
[13] Z. Chen and E. Bjornson, "Channel hardening and favorable propagation in cell-free massive MIMO with stochastic geometry," *IEEE Trans. Commun.*, vol. 66, no. 11, pp. 5205–5219, Nov. 2018.
[14] A. A. Polegre, F. Riera-Palou, G. Femenias, and A. G. Armada, "New insights on channel hardening in cell-free massive MIMO networks," in *Proc. IEEE Int. Conf. Commun. Workshops (ICC Workshops)*, Jun. 2020, pp. 1–6.
[15] L. Sanguinetti, E. Bjornson, and J. Hoydis, "Toward massive MIMO 2.0: Understanding spatial correlation, interference suppression, and pilot contamination," *IEEE Trans. Commun.*, vol. 68, no. 1, pp. 232–257, Jan. 2020.
[16] S. Gunnarsson, J. Flordelis, L. Van Der Perre, and F. Tufvesson, "Channel hardening in massive MIMO: Model parameters and experimental assessment," *IEEE Open J. Commun. Soc.*, vol. 1, pp. 501–512, 2020.
[17] H. Q. Ngo, H. Tataria, M. Matthaiou, S. Jin, and E. G. Larsson, "On the performance of cell-free massive MIMO in ricean fading," in *Proc. 52nd Asilomar Conf. Signals, Syst., Comput.*, Oct. 2018, pp. 980–984.
[18] J. Qiu, K. Xu, Z. Shen, W. Xie, D. Zhang, and X. Li, "Downlink performance analysis of cell-free massive MIMO over spatially correlated Rayleigh channels," in *Proc. IEEE 19th Int. Conf. Commun. Technol. (ICCT)*, Oct. 2019, pp. 122–127.
[19] W. Fan, J. Zhang, E. Bjornson, S. Chen, and Z. Zhong, "Performance analysis of cell-free massive MIMO over spatially correlated fading channels," in *Proc. IEEE Int. Conf. Commun. (ICC)*, May 2019, pp. 1–6.
[20] M. Zhou, Y. Zhang, X. Qiao, and L. Yang, "Spatially correlated Rayleigh fading for cell-free massive MIMO systems," *IEEE Access*, vol. 8, pp. 42154–42168, 2020.
[21] E. Bjornson and L. Sanguinetti, "Making cell-free massive MIMO competitive with MMSE processing and centralized implementation," *IEEE Trans. Wireless Commun.*, vol. 19, no. 1, pp. 77–90, Jan. 2020.
[22] O. Ozdogan, E. Bjoornson, and J. Zhang, "Cell-free massive MIMO with rician fading: Estimation schemes and spectral efficiency," in *Proc. 52nd Asilomar Conf. Signals, Syst., Comput.*, Oct. 2018, pp. 975–979.
[23] O. Ozdogan, E. Bjornson, and J. Zhang, "Performance of cell-free massive MIMO with rician fading and phase shifts," *IEEE Trans. Wireless Commun.*, vol. 18, no. 11, pp. 5299–5315, Nov. 2019.
[24] Y. Zhang, M. Zhou, H. Cao, L. Yang, and H. Zhu, "On the performance of cell-free massive MIMO with mixed-ADC under rician fading channels," *IEEE Commun. Lett.*, vol. 24, no. 1, pp. 43–47, Jan. 2020.
[25] S.-N. Jin, D.-W. Yue, and H. H. Nguyen, "Spectral and energy efficiency in cell-free massive MIMO systems over correlated rician fading," *IEEE Syst. J.*, early access, May 26, 2020, doi: 10.1109/JSYST.2020.2993048.
[26] S. Buzzi and C. D'Andrea, "User-centric communications versus cell-free massive MIMO for 5G cellular networks," in *Proc. 21th Int. ITG Workshop Smart Antennas*, Mar. 2017, pp. 1–6.
[27] S. Buzzi, C. D'Andrea, A. Zappone, and C. D'Elia, "User-centric 5G cellular networks: Resource allocation and comparison with the cell-free massive MIMO approach," *IEEE Trans. Wireless Commun.*, vol. 19, no. 2, pp. 1250–1264, Feb. 2020.
[28] E. Nayebi, A. Ashikhmin, T. L. Marzetta, H. Yang, and B. D. Rao, "Precoding and power optimization in cell-free massive MIMO systems," *IEEE Trans. Wireless Commun.*, vol. 16, no. 7, pp. 4445–4459, Jul. 2017.
[29] L. D. Nguyen, T. Q. Duong, H. Q. Ngo, and K. Tourki, "Energy efficiency in cell-free massive MIMO with zero-forcing precoding design," *IEEE Commun. Lett.*, vol. 21, no. 8, pp. 1871–1874, Aug. 2017.
[30] J. Zheng, J. Zhang, L. Zhang, X. Zhang, and B. Ai, "Efficient receiver design for uplink cell-free massive MIMO with hardware impairments," *IEEE Trans. Veh. Technol.*, vol. 69, no. 4, pp. 4537–4541, Apr. 2020.
[31] *Study on 3D channel model for LTE*, 3GPP, document 36.873 V12.0.0 Release 12, Technical Specification Group, 2014.
[32] E. Björnson, J. Hoydis, and L. Sanguinetti, "Massive MIMO networks: Spectral, energy, and hardware efficiency," *Found. Trends Signal Process.*, vol. 11, nos. 3–4, pp. 154–655, 2017, doi: 10.1561/2000000093.
[33] T. L. Marzetta, "Noncooperative cellular wireless with unlimited numbers of base station antennas," *IEEE Trans. Wireless Commun.*, vol. 9, no. 11, pp. 3590–3600, Nov. 2010.
[34] O. Elijah, C. Y. Leow, T. A. Rahman, S. Nunoo, and S. Z. Iliya, "A comprehensive survey of pilot contamination in massive MIMO–5G system," *IEEE Commun. Surveys Tuts.*, vol. 18, no. 2, pp. 905–923, 2nd Quart., 2016.
[35] H. Liu, J. Zhang, S. Jin, and B. Ai, "Graph coloring based pilot assignment for cell-free massive MIMO systems," *IEEE Trans. Veh. Technol.*, early access, Jun. 8, 2020, doi: 10.1109/TVT.2020.3000496.
[36] H. Liu, J. Zhang, X. Zhang, A. Kurniawan, T. Juhana, and B. Ai, "Tabu-Search-Based pilot assignment for cell-free massive MIMO systems," *IEEE Trans. Veh. Technol.*, vol. 69, no. 2, pp. 2286–2290, Feb. 2020.
[37] G. Femenias and F. Riera-Palou, "Cell-free millimeter-wave massive MIMO systems with limited fronthaul capacity," *IEEE Access*, vol. 7, pp. 44596–44612, 2019.
[38] S. M. Kay, *Fundamentals of Statistical Signal Processing: Estimation Theory*. Upper Saddle River, NJ, USA: Prentice-Hall, 1993.
[39] F. Riera-Palou, G. Femenias, A. G. Armada, and A. Perez-Neira, "Clustered cell-free massive MIMO," in *Proc. IEEE Globecom Workshops (GC Wkshps)*, Dec. 2018, pp. 1–6.
[40] E. Bjornson and L. Sanguinetti, "Scalable cell-free massive MIMO systems," *IEEE Trans. Commun.*, vol. 68, no. 7, pp. 4247–4261, Jul. 2020.
[41] I. Dokmanic, M. Kolundzija, and M. Vetterli, "Beyond Moore-penrose: Sparse pseudoinverse," in *Proc. IEEE Int. Conf. Acoust., Speech Signal Process.*, May 2013, pp. 6526–6530.
[42] O. Ozdogan, E. Bjornson, and E. G. Larsson, "Massive MIMO with spatially correlated rician fading channels," *IEEE Trans. Commun.*, vol. 67, no. 5, pp. 3234–3250, May 2019.
[43] X. Hu, C. Zhong, X. Chen, W. Xu, H. Lin, and Z. Zhang, "Cell-free massive MIMO systems with low resolution ADCs," *IEEE Trans. Commun.*, vol. 67, no. 10, pp. 6844–6857, Oct. 2019.
[44] B. Hassibi and B. M. Hochwald, "How much training is needed in multiple-antenna wireless links?" *IEEE Trans. Inf. Theory*, vol. 49, no. 4, pp. 951–963, Apr. 2003.
[45] H. Yang and T. L. Marzetta, "Capacity performance of multicell large-scale antenna systems," in *Proc. 51st Annu. Allerton Conf. Commun., Control, Comput. (Allerton)*, Oct. 2013, pp. 668–675.
[46] G. Interdonato, H. Q. Ngo, E. G. Larsson, and P. Frenger, "On the performance of cell-free massive MIMO with short-term power constraints," in *Proc. IEEE 21st Int. Workshop Comput. Aided Modeling Design Commun. Links Netw. (CAMAD)*, Oct. 2016, pp. 225–230.
[47] J. Zhang, E. Bjornson, M. Matthaiou, D. W. K. Ng, H. Yang, and D. J. Love, "Prospective multiple antenna technologies for beyond 5G," *IEEE J. Sel. Areas Commun.*, early access, Jun. 1, 2020, doi: 10.1109/JSAC.2020.3000826.

ALBERTO ÁLVAREZ POLEGRE (Student Member, IEEE) received the M.Sc. degree in telecommunication engineering from the University of Las Palmas de Gran Canaria (ULPGC), Las Palmas, Spain, in 2015. He is currently pursuing the Ph.D. degree with the Communications Research Group, Universidad Carlos III de Madrid (UC3M). From November 2015 to March 2017, he was with GMV as a Software Engineer for aircraft communications development and testing. He has been a part of the OPALL5G (Small Cells Performance Optimization in 5G NR Networks) Project jointly developed with Nokia Spain. His current research interests include interference management in wireless communication networks, 5G and massive MIMO systems, and cell-free massive MIMO deployments.

FELIP RIERA-PALOU (Senior Member, IEEE) received the B.S./M.S. degree in computer engineering from the University of the Balearic Islands (UIB), Mallorca, Spain, in 1997, the M.Sc. and Ph.D. degrees in communication engineering from the University of Bradford, U.K., in 1998 and 2002, respectively, and the M.Sc. degree in statistics from The University of Sheffield, U.K., in 2006. From May 2002 to March 2005, he was with Philips Research Laboratories, Eindhoven, The Netherlands, first as a Marie Curie Postdoctoral Fellow (European Union) and later as a Member of Technical Staff. While at Philips, he worked on research programs related to wideband speech/audio compression and speech enhancement for mobile telephony. From April 2005 to December 2009, he was a Research Associate (Ramon y Cajal program, Spanish Ministry of Science) at the Mobile Communications Group, Department of Mathematics and Informatics, UIB, where he has been an Associate Research Professor (I3 Program, Spanish Ministry of Education), since January 2010. His current research interests include signal processing and wireless communications.

GUILLEM FEMENIAS (Senior Member, IEEE) received the Telecommunication Engineer degree and the Ph.D. degree in electrical engineering from the Technical University of Catalonia (UPC), Barcelona, Spain, in 1987 and 1991, respectively. From 1987 to 1994, he was a Researcher with UPC, where he became an Associate Professor, in 1992. In 1995, he joined the Department of Mathematics and Informatics, University of the Balearic Islands (UIB), Mallorca, Spain, where he became a Full Professor, in 2010, and is currently leading the Mobile Communications Group, where he has been the Project Manager of the projects ARAMIS, DREAMS, DARWIN, MARIMBA, COSMOS, ELISA, and TERESA, all of them funded by the Spanish and Balearic Islands Governments. In the past, he was also involved with several European projects (ATDMA, CODIT, and COST). His current research interests and activities include digital communications theory and wireless communication systems, with a particular emphasis on radio resource management strategies applied to 5G and 6G wireless networks. On these topics, he has published more than 100 journal articles and conference papers, as well as some book chapters. He was a recipient of the Best Paper Awards at the 2007 IFIP International Conference on Personal Wireless Communications and the 2009 IEEE Vehicular Technology Conference-Spring. He has served for various IEEE conferences as a Technical Program Committee Member, as the Publications Chair for the IEEE 69th Vehicular Technology Conference (VTC-Spring 2009), and as a Local Organizing Committee Member of the IEEE Statistical Signal Processing (SSP 2016).

ANA GARCÍA ARMADA (Senior Member, IEEE) received the Ph.D. degree in electrical engineering from the Polytechnical University of Madrid, in February 1998. She has been a Visiting Scholar with Stanford University, Bell Labs, and the University of Southampton. She is currently a Professor with the Universidad Carlos III de Madrid, Spain, where she is leading the Communications Research Group. She has coauthored eight book chapters on wireless communications and signal processing. She has published around 150 articles in international journals and conference proceedings. She holds four patents. She has participated (coordinated most of them) in more than 30 national and 10 international research projects as well as 20 contracts with the industry, all of them related to wireless communications. Her main research interests include multicarrier and multiantenna techniques, and signal processing applied to wireless communications. She has contributed to international standards organizations, such as ITU and ETSI, and is a member of the expert group of the European 5G PPP and the Advisory Committee 5JAC of the ESA, as an Expert appointed by Spain on 5G. She has served on the TPC of more than 40 conferences. She was a part of the Organizing Committee of the IEEE 5G Summit 2017 and the IEEE Vehicular Technology Conference (VTC) Fall 2018, Spring 2018, and 2019, among others. She will be a part of the Organizing Committee of the IEEE GLOBECOM, in 2021 (General Chair). She was the Secretary of the IEEE ComSoc Women in Communications Engineering Standing Committee, from 2016 to 2017, where she was the Chair, from 2018 to 2019. She was the Newsletter Editor of the IEEE ComSoc Signal Processing and Consumer Electronics Committee, from 2017 to 2018, where she has been the Secretary, since 2019. She received the Young Researchers Excellence Award, the Award to Outstanding Achievement in Research, Teaching, and Management, and the Award to Best Practices in Teaching, all from the Universidad Carlos III de Madrid. She received the Exemplary Editor Award, in 2017 and 2018. She received the Third Place Bell Labs Prize 2014 for shaping the future of information and communications technology. She also received the Outstanding Service Award from the IEEE ComSoc Signal Processing and Communications Electronics (SPCE) Technical Committee, in 2019. She has served on the Editorial Board of *Physical Communication*, from 2008 to 2017, and *IET Communications*, from 2014 to 2017. She served on the Editorial Board of the IEEE COMMUNICATIONS LETTERS as an Editor, from 2016 to February 2019, and as a Senior Editor, from 2016 to March 2019, and has been serving on the Editorial Board of the IEEE TRANSACTIONS ON COMMUNICATIONS, since 2019.